

AD-A085 161

ATLANTIC RESEARCH CORP ALEXANDRIA VA F/G 20/14
COMMUNICATIONS-ELECTRONIC INTRASYSTEM ELECTROMAGNETIC INTERFERE--ETC(U)
MAY 80 L E POLISKY, J SAVAGE DAAK80-79-C-0786

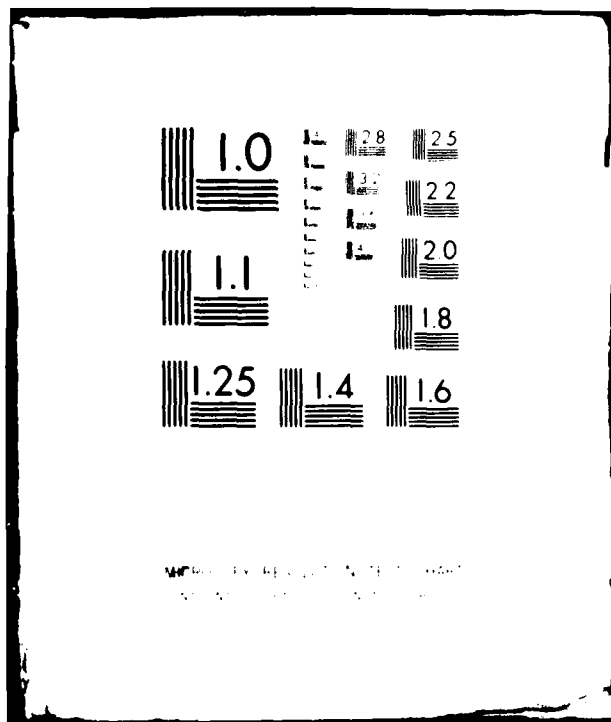
UNCLASSIFIED

CORADCOM-79-0786-3

NL

1-1
A
2 28.00

END
DATE
FILMED
7 80
DTIC



ADA085161



LEVEL *HH*

AOE18-0 5

(12)

RESEARCH AND DEVELOPMENT TECHNICAL REPORT
CORADCOM-79-0786-3

COMMUNICATIONS - ELECTRONIC INTRASYSTEM
ELECTROMAGNETIC INTERFERENCE MEASUREMENT
TECHNIQUES AND INSTRUMENTATION

Lester E. Polisky and John Savage
ATLANTIC RESEARCH CORPORATION
5390 Cherokee Avenue
Alexandria, Virginia 22314

DTIC
COLLECTED
JUN 4 1980

May 1980

Quarterly Report for Period 21 December 1979 -
20 March 1980

Approved for public release: Distribution unlimited

Prepared for: CENCOMS

CORADCOM
US ARMY COMMUNICATIONS RESEARCH & DEVELOPMENT COMMAND
FORT MONMOUTH, NEW JERSEY 07703

80 6 3 029

DDC FILE COPY

NOTICES

Disclaimers

The citation of trade names and names of manufacturers in this report is not to be construed as official Government indorsement or approval of commercial products or services referenced herein.

Disposition

Destroy this report when it is no longer needed. Do not return it to the originator.



RESEARCH AND DEVELOPMENT TECHNICAL REPORT
CORADCOM-79-0786-3

**COMMUNICATIONS - ELECTRONIC INTRASYSTEM
ELECTROMAGNETIC INTERFERENCE MEASUREMENT
TECHNIQUES AND INSTRUMENTATION**

**Lester E. Polisky and John Savage
ATLANTIC RESEARCH CORPORATION
5390 Cherokee Avenue
Alexandria, Virginia 22314**

May 1980

**Quarterly Report for Period 21 December 1979 -
20 March 1980**

Approved for public release: Distribution unlimited

Prepared for: CENCOMS

CORADCOM
US ARMY COMMUNICATIONS RESEARCH & DEVELOPMENT COMMAND
FORT MONMOUTH, NEW JERSEY 07703

UNCLASSIFIED

SECURITY CLASSIFICATION OF THIS PAGE (When Data Entered)

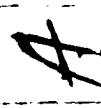
REPORT DOCUMENTATION PAGE		READ INSTRUCTIONS BEFORE COMPLETING FORM
1. REPORT NUMBER (18) CORADCOM-79-0786-3/	2. GOVT ACCESSION NO. AD-A085161	3. RECIPIENT'S CATALOG NUMBER (no. 3)
4. TITLE (and Subtitle) (6) Communications-Electronic Intrasytem Electromagnetic Interference Measurement Techniques and Instrumentation.	5. TYPE OF REPORT & DATES COVERED (9) Quarterly Report 21 Dec 1979- 20 March 1980	6. PERFORMING ORG. REPORT NUMBER
7. AUTHOR(s) (10) Lester E./Polisky John/Savage	8. CONTRACT OR GRANT NUMBER(s) (15) DAAK80-79-C-0786	
9. PERFORMING ORGANIZATION NAME AND ADDRESS Atlantic Research Corporation 5390 Cherokee Ave. Alexandria, Va 22314	10. PROGRAM ELEMENT, PROJECT, TASK AREA & WORK UNIT NUMBERS	
11. CONTROLLING OFFICE NAME AND ADDRESS CORADCOM ATTN: DRDCO-COM-RY-3 Ft. Monmouth, NJ 07703	12. REPORT DATE (11) May 1980	13. NUMBER OF PAGES 67
14. MONITORING AGENCY NAME & ADDRESS (if different from Controlling Office) (12) 73	15. SECURITY CLASS. (of this report) Unclassified	16. DECLASSIFICATION/DOWNGRADING SCHEDULE
16. DISTRIBUTION STATEMENT (of this Report) Approved for public release Distribution Unlimited		
17. DISTRIBUTION STATEMENT (of the abstract entered in Block 20, if different from Report)		
18. SUPPLEMENTARY NOTES		
19. KEY WORDS (Continue on reverse side if necessary and identify by block number)		
20. ABSTRACT (Continue on reverse side if necessary and identify by block number) This report presents the results obtained during the third quarter of the Communications-Electronics Intrasytem Electromagnetic Interference Measurement Techniques and Instrumentation Project. The period covered was 21 Dec. 1979 to 20 March 1980. The major effort in the third quarter consisted of completing the broadband measurement technique description and initiating the evaluation of MIL-STD-461 A techniques. 045550 Ju		

DD FORM 1 JAN 73 1473 EDITION OF 1 NOV 65 IS OBSOLETE

UNCLASSIFIED
SECURITY CLASSIFICATION OF THIS PAGE (When Data Entered)

Table of Contents

<u>Section</u>	<u>Page</u>
1. Introduction	1
2. Third Quarter Events	2
3. Work Accomplished in Third Quarter	3
A. Broadband Measurements of Emission	3
1) Improved Broadband Measurement System	4
a) Wide Dynamic Range Detectors	5
b) Dynamic Range Improvement	16
c) Broadband Measurement System, Second Cut	25
2) Experimental Verification	28
a) Detector Conversion Response	28
(1) CW Detailed Analysis	35
(2) Impulse Detailed Analysis	36
(3) Noise Detailed Analysis	37
(4) Revised Detector Conversion Response Predictions	41
b) Bandwidth Factors	44
(1) Effect of Bandwidth on Noise	44
(2) Effect of Bandwidth on Impulses	47
3) Broadband Measurement System Conclusions	52
B. Evaluation of MIL-STD-461A Limits and Measurement Procedure	54
1) Background	54
2) Class IIIA Systems	54
3) Class I and Class II Equipment	54
4) Intra System Testing and Analysis	56
4. Work Planned for Fourth Quarter	58

Accession For	N110 0001	DDC TAB	Unannounced	Justification
By	Date	Avail	Dist	
				

1. INTRODUCTION

This is the third of three quarterly reports submitted under this contract. The purpose of this contract is to develop an improved approach to the communication-electronic system integration investigating the use of computerized analytical tools such as IEMCAP in conjunction with the overall EMI test procedures of MIL-STD-461A and 462 to develop a more meaningful and economical approach to defining the system EMI problems. The analytical techniques provide guidance and insight into system characteristics that will allow for effective utilization of measurement resources and time. The contract results will lead to the establishment of an interactive EMI/EMC analysis and measurement procedure that will provide the basis for a meaningful EMI intrasystem measurement standard. In pursuit of the contract goals, this quarterly report contains a description of broadband measurement techniques and an evaluation of the required EMI/EMC test procedures and limits.

This is a four section report. In addition to this introductory section, Section 2 describes third quarter events, Section 3 describes the work accomplished in the third quarter and Section 4 describes the work planned for the final quarter of the project.

2. THIRD QUARTER EVENTS

Third quarter events included a meeting at USACORADCOM on 14 February 1980 which concentrated technical effort in two major project areas. They were the completion of the broadband measurement technique development and the evaluation of the MIL-STD-461A test procedures and limits.

The 14 February meeting allowed Atlantic Research project personnel to consult with USACORADCOM personnel on the broadband measurement technique effort and some proposed changes to MIL-STD-461A limits based on EMI/EMC computer analysis which would be performed prior to MIL-STD-461A testing of a system and the use of the broadband measurement techniques that were being developed for the EMI/EMC testing. Additionally, the second quarterly report was discussed since it contained a great deal of this information. In attendance at the meeting were:

USACORADCOM	- Warren Kesselman
	- Paul Major
	- Stuart Albert
Atlantic Research	- William Duff
	- Lester Polisky
	- John Savage

3. WORK ACCOMPLISHED IN THIRD QUARTER

The work in the third quarter has completely defined a broadband emission measurement technique from 14 kHz to 10 GHz and has produced an initial evaluation of the MIL-STD-461A limits and MIL-STD-462 measurement procedures.

For MIL-STD-461A defined Class IIIA equipments the broadband emission measurement technique will be directly applicable since only emission tests are required. They are RE05 and CE03. However, for intrasystem EMI/EMC testing of Class IIIA equipments or EMI/EMC testing of Class I or Class I equipments broadband measurement techniques may only be applied for some of the required measurements. The same condition applies to automated measurement techniques. Broadband and automated measurement techniques are not amenable to some of the MIL-STD-462 measurement procedures. Table 12 lists these measurements. In the fourth quarter this problem will be examined further and alternative test techniques suggested where possible.

A. Broadband Measurements of Emission

In the previous Quarterly Report, a hypothetical Broadband Measurement System based on a crystal-video receiver and broadband antennas was analyzed for factors affecting its practical realization. Expressions were presented for sensitivity to CW and impulse signals in the presence of receiver noise. The sensitivity was shown to be adequate for MIL-STD-461-type measurements. The concept was then advanced that an impulse-to-CW response ratio can be specified by controlling the post-detection to pre-detection bandwidth ratio, and that the response to all other types of signals will fall somewhere between the CW and impulse responses. This concept was used to generate a hypothetical Broadband Measurement Specification reflecting suitable changes in the RE02 limits. Examination of the impulse levels that would have to be handled in the hypothetical system during measurements to the new limits revealed that an impractical detector drive level of hundreds of peak watts would be required to provide sufficient dynamic range.

This Quarterly Report finds a solution (up to 1 GHz) to the dynamic range problem in improved state-of-the-art detector sensitivity and reduction of RF gain to provide detector-noise-limited operation as opposed to input-noise-limited operation. The gain reconfiguration results in generation of a second-cut hypothetical Broadband Measurement System block diagram. Results of laboratory measurements using CW (representing the simplest narrowband signal), white noise (representing worst-case uncorrelated broadband signals) and impulses (representing worst-case correlated broadband signals) are then presented to verify the mathematics of the previous Quarterly Report. A discrepancy in the noise verification leads to an improved mathematical model for the handling of noise by the detector. Finally, criteria for a realizable Broadband Measurement System are set forth.

1) Improved Broadband Measurement System

The hypothetical Broadband Measurement System presented in the previous Quarterly Report suffered from inadequate dynamic range to handle worst-case impulse signals. The thought of improving the situation by using several detectors in series with progressively smaller bandwidths between them was quickly abandoned when it was realized that the dynamic range requirement is squared in every square-law detector through which the signal passes. Other standard dynamic range extension means such as feedback linearization, logarithmic amplification and progressive detection are out of the question because of the extremely wide bandwidths required. Breaking up the five bands into subbands for parallel analysis is workable but would complicate the system and probably make it prohibitively expensive.

The dynamic range problem focusses on the detector. The RF amplifiers preceeding the detector will have sufficient dynamic range if their gains can be reduced. The gains are excessive because the detector is not sensitive enough alone. A simple solution presents itself if the detector sensitivity can be improved and/or other means found to reduce the RF amplifier gain required.

a) Wide Dynamic Range Detectors

Up to this point, the detectors used in the hypothetical Broadband Measurement System have been assumed to have a nominal -55 dBm tangential sensitivity. Driven by typical amplifiers with +13 to +29 dBm output capability, this leads to dynamic ranges of 68 to 84 dB. Dynamic ranges of 70 to 100 dB are required if the system is to function with $r=20$ dB as intended, where r is the broadband to narrow band response ratio.

Further investigation of diode detector technology discloses that low-barrier Schottky detector diodes are not available from Hewlett-Packard with voltage sensitivities as high as 30 mV/ μ W (compared with 0.4 mV/ μ W for the older point-contact diodes.) Investigation also discloses that tangential sensitivity is a complex function of diode voltage sensitivity, bandwidth, bias and 1/f noise. A considerable improvement in dynamic range can be affected if calculated tangential sensitivity values are used in the system performance evaluation instead of nominal values.

Tangential sensitivity, T_{SS} , for a detector is commonly defined as the signal input required for an output signal-to-noise ratio of 8 dB. Thus:

$$V_{SO} - V_{NO} = 8 \text{ dB}$$

where V_{SO} is the RMS signal output voltage and V_{NO} is the RMS noise output voltage, both in dB μ V for a CW (or non-bandwidth-limited pulse) input signal.

Typical data from Hewlett-Packard describing low-barrier Schottky diodes optimized for detector usage show a dynamic transfer characteristic with a square-law region at low signal levels and a linear region at high signal levels, which is typical of most detector diodes.

In the square-law region:

$$V_O = \frac{\gamma R_O P_I}{R_O + R_V} \quad (1)$$

where γ is the voltage sensitivity of the diode in mV/ μ W, R_O is the detector output load resistance in ohms, R_V is detector diode internal video resistance in ohms, P_I is signal power input in μ W

and V_0 is detected signal output in mV. A lossless return path is assumed to exist for the video through the RF source.

Converting to decibels and standardizing units with a 50-ohm input, Equation (1) becomes:

$$\begin{aligned} 20 \log_{10} V_{SO} &= 20 \log_{10} (10^{-3}) + 20 \log_{10} \frac{R_0}{R_0 + R_V} \\ &+ 20 \log_{10} \frac{V_{SI}^2}{50}, \text{ from which} \\ V_{SO} &= 20 \log_{10} (10^{-3}) + 20 \log_{10} \frac{R_0}{R_0 + R_V} + 2V_{SI} - 94 \text{ dB}\mu\text{V} \end{aligned} \quad (2)$$

where V_{SO} and V_{SI} are in dB μ V.

There are two noise sources associated with V_{NO} : thermal noise in R_0 , and shot and flicker noise in R_V . Since R_0 must be small in comparison to R_V in order to realize the wide bandwidth required by an average-responding detector, R_0 will determine the source resistance seen by the video amplifier and the noise voltage, e_{RO} , contributed by R_0 and the video amplifier will be:

$$e_{RO} = \sqrt{4kTB_0 R_0 F} \quad (3)$$

where $4kTB_0$ is the thermal noise power generated in output bandwidth B_0 and F is the noise figure of the output video amplifier.

The diode video resistance, R_V , contributes both shot noise which has a flat frequency characteristic and excess flicker noise which has a $1/f$ characteristic. There is also some thermal noise in the connection resistance component of R_V , but this is generally negligible in comparison with shot and flicker noise in the barrier resistance. Since the detector must operate down to DC, flicker noise is important in this application. Fortunately, detector diodes for doppler radar must operate at low video frequencies so considerable attention has been paid to controlling flicker noise in recently developed diodes. The noise voltage, e_{RV} , contributed by R_V will be:

$$e_{RV} = \sqrt{4kTB_0 R_V t_d} \quad (4)$$

where t_d is the diode noise temperature ratio. It is interesting to note that t_d can be less than unity for Schottky diodes in the absence of flicker noise (i.e., at high video frequencies).¹

1. A. M. Cowley and H. O. Sorensen: "Quantitative Comparison of Solid-State Microwave Devices." IEEE Transaction on MTT, Vol. 14, No. 12, December 1966.

The RMS sum of e_{R_O} and e_{R_V} at the video amplifier input from the equivalent circuit in Figure 1 is:

$$V_{NO}^2 = \left[\frac{e_{R_O} R_V}{R_O + R_V} \right]^2 + \left[\frac{e_{R_V} R_O}{R_O + R_V} \right]^2$$

$$V_{NO} = \frac{\sqrt{4kTB_O (R_O R_V^2 F + R_V R_O^2 t_d)}}{R_O + R_V}$$

$$= \frac{2\sqrt{R_O R_V} \sqrt{kTB_O (R_V F + R_O t_d)}}{R_O + R_V} \quad (5)$$

Converting to decibel notation:

$$V_{NO} = 20 \log_{10} \frac{2\sqrt{R_O R_V}}{R_O + R_V} + 10 \log_{10} kTB_O + 10 \log_{10} (R_V F + R_O t_d) \quad (6)$$

For tangential sensitivity $V_{SI} = T_{ss}$ and

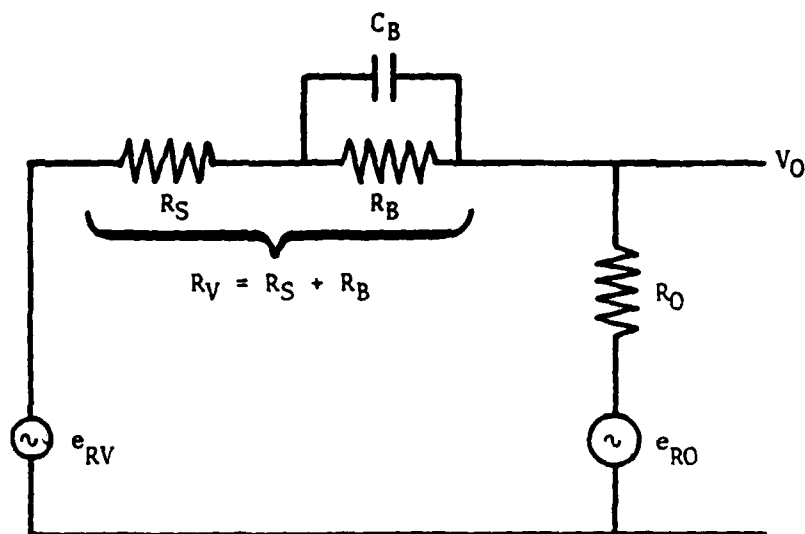
$$2T_{ss} = (V_{NO} + 8) - 20 \log_{10} \gamma - 20 \log_{10} \frac{R_O}{R_O + R_V} + 94$$

$$= 102 + 20 \log_{10} \frac{2\sqrt{R_O R_V}}{R_O + R_V} + 10 \log_{10} kTB_O + 10 \log_{10} (R_V F + R_O t_d)$$

$$- 20 \log_{10} \gamma - 20 \log_{10} \frac{R_O}{R_O + R_V}$$

$$T_{ss} = 12.1 + 5 \log_{10} B_O + 5 \log_{10} \left[\frac{R_V^2 F}{R_O} + R_V t_d \right] - 10 \log_{10} \gamma + C_f \text{ dB} \quad (7)$$

where C_f is an RF input frequency correction factor in dB.



R_S = diode connection resistance

R_B = diode barrier resistance

C_B = diode barrier capacitance

R_O = video amplifier input resistance

e_{RV} = diode noise voltage

e_{RO} = video amplifier equivalent input noise voltage

Figure 1. Detector Equivalent Circuit.

Selecting the Hewlett-Packard 5082-2824 diode for use below 1 GHz because of its low flicker noise and high reverse voltage rating provides values of $R_V = 1500$ ohms and $\gamma = 6$ mV/ μ W for band 1 and 2 of the Wideband Measurement system hypothesized in the previous Quarterly Report. Selecting the 5082-2755 diode for use above 1 GHz because of its wide frequency response provides values of $R_V = 1500$ ohms and $\gamma = 5$ mV/ μ W for Bands 3 through 5.

Values of diode temperature ratio, t_d , were obtained by replotting catalog data provided by Hewlett-Packard and extrapolating down to the low video frequencies required by the Wideband Measurement System as shown in Figure 2. The extrapolation assumes that flicker noise power increases inversely with frequency in accordance with the relationship

$$\Delta t_d = 1 + \frac{f_N}{f_0} \quad (8)$$

where f_N is the flicker noise corner frequency (3 dB point on excess noise curve) and f_0 is the incremental video output frequency. Integrating Δt_d between the lower edge, f_L , and the upper edge, f_U , of the video output bandwidth, B_0 , results in the following expression for the effective noise temperature ratio, t_d , within the output bandwidth:

$$\begin{aligned} t_d &= \int_{f_L}^{f_U} \left(1 + \frac{f_N}{f_0} \right) df_0 \\ &= \int_{f_L}^{f_U} df_0 + f_N \int_{f_L}^{f_U} \frac{df_0}{f_0} \end{aligned}$$

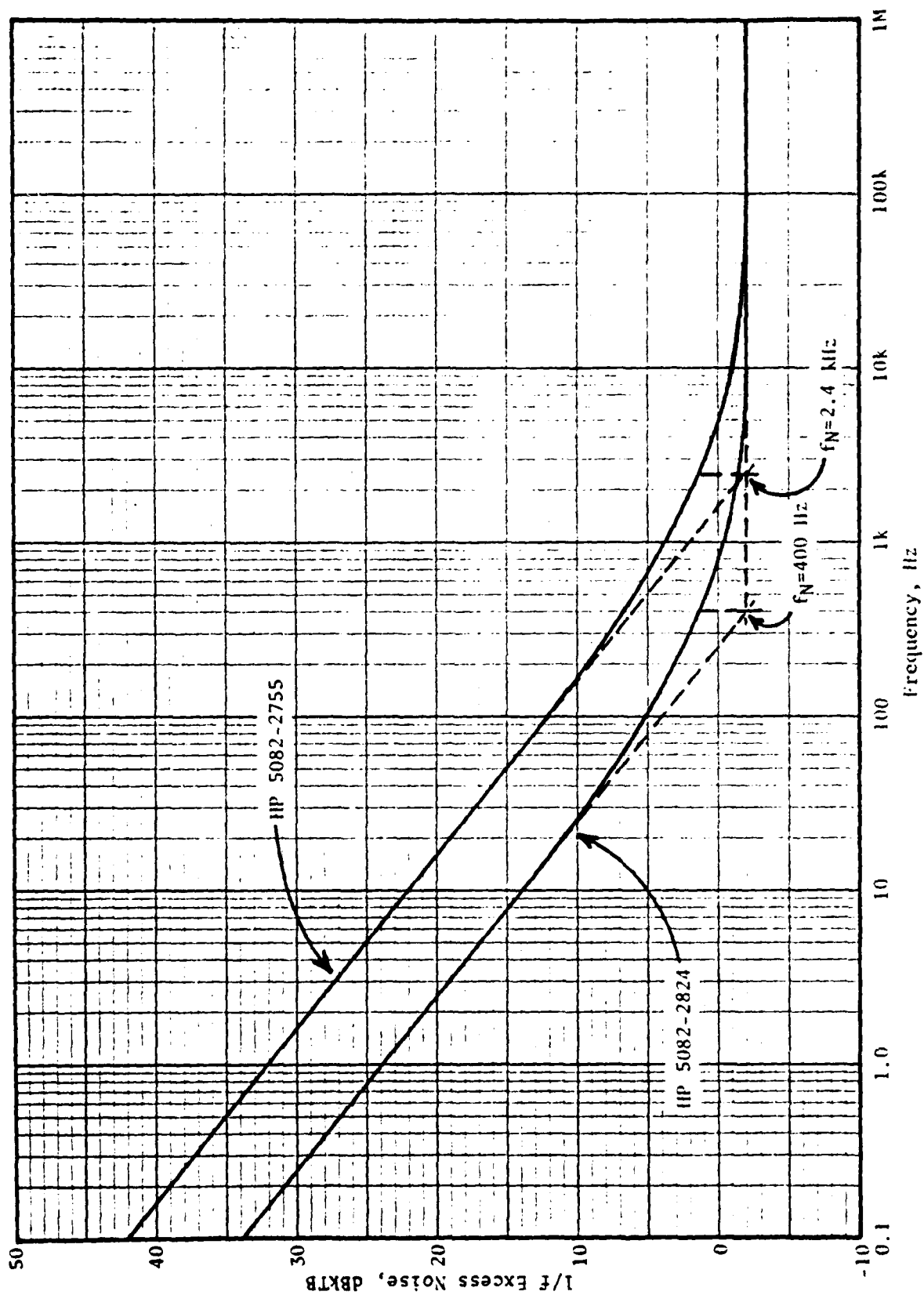


Figure 2. Diode Flicker Noise, 25°C, 20μA Bias.

$$t_d = f_U - f_L + f_N (\ln f_U - \ln f_L)$$

$$t_d = f_U - f_L + f_N \ln(f_U/f_L)$$

$$B_0 = f_U - f_L$$

$$t_d = B_0 + f_N \ln\left(\frac{B_0}{f_L} + 1\right) \quad (9)$$

From Figure 2, the flicker noise corner frequency for the HP 5082-2755 diode is 2.4 kHz, and for the HP 5082-2824 diode is 400 Hz. The effective noise temperature ratio for the latter diode used in Band 1 of the hypothetical Broadband Measurement System is thus:

$$t_d = B_0 + f_N \ln\left(\frac{B_0}{f_L} + 1\right)$$

$$= 50 + 400 \ln\left(\frac{50}{1} + 1\right)$$

$$= 1623$$

$$t_d = 32.1 \text{ dB}$$

Values of t_d for the various bands in the hypothetical Broadband Measurement System are listed in Table 1.

Table 1.

Diode Noise Temperature Ratios For Hewlett-Packard 5082-2755 Diode

<u>Band</u>	<u>Frequency</u>	<u>Video Output Bandwidth, B_o</u>	<u>Diode Noise Corner, f_N</u>	<u>Diode Temperature Ratio, t_d</u>
1	10kHz-100MHz	50Hz	2400Hz	39.8 dB
2	100-1000MHz	5.5	2400	36.5
3	1-4GHz	1.7	2400	33.8
4	4-7	1.7	2400	33.8
5	7-10	1.7	2400	33.8

Diode Noise Temperature Ratios for Hewlett-Packard 5082-2824 Diode

<u>Band</u>	<u>Frequency</u>	<u>Video Output Bandwidth, B_o</u>	<u>Diode Noise Corner, f_N</u>	<u>Diode Temperature Ratio, t_d</u>
1	10kHz-100MHz	50Hz	400Hz	32.1dB
2	100-1000MHz	5.5	400	28.8
3	1-4 GHz	1.7	400	26.0
4	4-7	1.7	400	26.0
5	7-10	1.7	400	26.0

Although the output of the detector will be DC coupled, f_L has been taken as 1 Hz in the above calculation so that the results will be determinate. A value of $f_L = 0$ leads to a prediction of infinite noise near DC which does not agree with reality. A value of $f_L = 1$ Hz assumes that the flicker noise contribution below 1 Hz will be negligible. Because the hypothetical Broadband Measurement System operates with video output bandwidths of only a few hertz, the accuracy of this assumption is fairly critical and should be the subject of further study.

A correction, C_f , for the falloff in T_{ss} at high microwave frequencies due to junction capacitance effects was obtained from Hewlett-Packard catalog data, extrapolating where necessary.²

The tangential sensitivity for Band 1 was calculated using Equation (7) as:

$$\begin{aligned}
 T_{ss} &= 12.1 + 5 \log_{10} B_0 + 5 \log_{10} \left[\frac{R_V^2 F}{R_0} + R_V t_d \right] - 10 \log_{10} 3 + C_f \\
 &= 12.1 + 5 \log_{10} 50 + 5 \log_{10} \left[\frac{1500^2 (2)}{50} + 1500 (1623) \right] \\
 &\quad - 10 \log_{10} 6 + 0 \\
 &= 12.1 + 8.5 + 32.0 - 7.8 + 0 \\
 &= 44.8 \text{ dB}\mu\text{V}
 \end{aligned}$$

Examination of the third term in the above equation discloses that diode flicker noise is 27 times amplifier input noise. A considerable improvement in T_{ss} could be realized if flicker noise could be reduced by reducing bias current, but the increase in R_V accompanying the decrease in bias current results in a net loss in T_{ss} . Calculated values of T_{ss} are listed for the two diodes in Table 2.

2. "Diode and Transistor Designer's Catalog" Hewlett-Packard Components, 1980, p. 110.

Table 2.

Calculated Tangential Sensitivity

For Hewlett-Packard 5082-2755 Diode

<u>Band</u>	<u>Frequency</u>	<u>B_o</u>	<u>γ</u>	<u>t_d</u>	<u>C_f</u>	<u>T_{ss}</u>	
						<u>Voltage</u>	<u>Wattage</u>
1	10kHz-100MHz	50Hz	5uV/ μ W	39.8dB	0dB	49.4dB μ V	-57.6dBm
2	100-1000MHz	5.5	5	36.5	0	43.0	-64.0
3*	1-4 GHz	1.7	5	33.8	0	39.1	-67.9
4*	4-7 GHz	1.7	5	33.8	1	40.1	-66.9
5*	7-10 GHz	1.7	5	33.8	3	42.1	-64.9

For Hewlett-Packard 5082-2824 Diode

<u>Band</u>	<u>Frequency</u>	<u>B_o</u>	<u>γ</u>	<u>t_d</u>	<u>C_f</u>	<u>T_{ss}</u>	
						<u>Voltage</u>	<u>Wattage</u>
1*	10kHz-100MHz	50Hz	6mV/ μ W	32.1dB	0dB	44.8dB μ V	-62.2dBm
2*	100-1000MHz	5.5	6	28.8	1.3	39.8	-67.2
3	1-4GHz	1.7	6	26.0	5.2	39.9	-67.1
4	4-7GHz	1.7	6	26.0	9.1	43.8	-63.2
5	7-10GHz	1.7	6	26.0	13.0	47.7	-59.3

*Selected for use in the Broadband Measurement System

The detector diodes used in the above calculations were assumed to be biased with 20 μ A of DC current to achieve the results indicated. This bias current is optimum for operation at an RF input frequency of 10 GHz. More complete data³ indicates that flicker noise corner frequency varies directly with bias current and shot noise increases with bias current. A few dB improvement over the T_{ss} values in Table 2 is probably possible by optimizing bias current for each band, instead of using a fixed value of 20 μ A.

Schottky diodes intended for zero-bias operation are also available from Hewlett-Packard, but no noise data is presented in the catalog. Elimination of bias current should eliminate flicker noise and greatly improve T_{ss} for DC-coupled detectors. Unfortunately, video resistances tend to be much higher than for biased diodes, although the 2000-8000 ohms shown for some newer types is a considerable improvement over early types that had video resistances on the order of a megohm. Tangential sensitivities and voltage sensitivities for the new diodes are quite good, coming within a couple of dB of biased diodes. Very low reverse breakdown voltages, on the order of 0.2 volt, tend to prevent their application in systems requiring wide dynamic range as are being analyzed here.

3. Application Note 923, Hewlett-Packard.

b) Dynamic Range Improvement

The calculated tangential sensitivity (T_{ss}) values listed in Table 2 are a considerable improvement over the nominal value of -55 dBm used previously. Assuming that the system can achieve a satisfactory false alarm rate (a false alarm would be a tripping of the go/no-go indicator in the absence of emissions above the new specification limits) with input levels equal to T_{ss} , optimum use can be made of the improvement by changing the RF amplifier gains in the hypothetical Broadband Measurement System so that narrowband signals at the new specification limits (Hypothetical Broadband Measurement Specification, First Cut, Figure 6 of second Quarterly Report) reach the detectors at levels just equal to T_{ss} . The required gains, calculated as $T_{ss} - (\text{Specification Limit Field Strength in dB}\mu\text{V/m}) + (\text{Antenna Factor in dB/m})$, are listed in Table 3 over the frequency range of interest. The new choice of amplifiers is shown in Table 4. The gains selected, which come as close as possible to the required values with commercial amplifiers meeting the requirements for frequency coverage and power output, are considerably reduced from those used in the first-cut system. RF amplifier noise figure is now of secondary importance because the new specification limits are substantially above the system noise floor. Because RF amplifier gains are no longer sufficient to raise RF input noise up to the detector thresholds, the system sensitivity is now detector/video-amplifier noise limited.

The improved dynamic ranges and the data used in their calculation are listed for each band in Table 5. Starting with the voltages produced at the terminals of antennas immersed in narrowband (CW) fields at the new specification limits, the RF amplifier gains were added and then attenuated until the detector inputs just equaled T_{ss} . The dynamic ranges for CW were calculated by subtracting T_{ss} from the RF amplifier (saturation) or detector (voltage breakdown) overload point, whichever was lower.

Table 3. CW Input Levels At Hypothetical Specifiaion Limit

<u>Band</u>	<u>Frequency</u>	<u>Narrowband Spec. Limit Field Strength</u>	<u>Antenna Factor</u>	<u>CW Ant. Output</u>	<u>Detector Tss</u>	<u>Gain Required</u>
1	10kHz	30dB μ V/m	6dB/m	24dB μ V	44.8dB μ V	20.8dB
	10MHz	30	6	24	44.8	20.8
	100	30	8	22	44.8	20.8
2	100MHz	30	8	22	39.8	17.8
	150	33	5	28	39.8	11.8
	200	36	8	28	39.8	11.8
	400	42	14	28	39.8	11.8
	800	48	20	28	39.8	11.8
	1000	50	22	28	39.8	11.8
3	1GHz	50	26	24	39.1	15.1
	4	62	39	23	39.1	16.1
4	4	62	39	23	39.1	16.1
	7	67	44	23	40.1	17.1
5	7	67	44	23	40.1	17.1
	10	70	47	23	42.1	19.1

Table 4.
Wideband Amplifier Characteristics

<u>Band</u>	<u>Manufacturer</u>	<u>Model</u>	<u>+ 1dB Frequency Response</u>	<u>Gain</u>	<u>Noise Figure</u>	<u>Power Output</u>	<u>Total Gain</u>
1	Avantek	UA-303(2)	.002-300 MHz	7x2 dB	9 dB	12 dBm	
1	Avantek	UA-304	.002-300	7	11	17	21 dB
2	Avantek	UA-405	20-1000	11	10	20	
2	Avantek	UA-408	10-1000	9	12	26	20
3	Avantek	AMG-4053	1-4 GHz	25	4.8	15	25
4	Avantek	AMT-8053	4-8	19	6.0	20	19
5	Avantek	AMT-12033	7-12	22	5.5	15	22

Table 5. Dynamic Range

Band	Spec. Limit CW Ant. Out.	Amplifier Gain	Amp. Out. w/o Atten.	Detector Tss	Atten. In. Amp. In.	Atten. Required Amp. Out.	Overload Point Amplifier	Overload Point Detector
1	24dB μ V	21dB	45dB μ V	45dB μ V	0dB	0dB	124 dB μ V	134dB μ V
2	28	20	48	40	8	0	133	134
3	23	25	48	39	9	0	122	125
4	23	19	42	40	0	2	127	125
5	23	22	45	42	3	0	122	125

Band	Frequency	Spec. Limit Imp. Ant. Out.	20 Log ₁₀ RF BW	Spec. Lim. Det. In. CW	Spec. Lim. Det. In. Impulse	Dynamic Range CW	Dynamic Range Impulse
1	10kHz-100MHz	44dB μ V/MHz	40dB	45dB μ V	105dB μ V	79dB	19dB
2	100-1000MHz	48	59	40	119	93	14
3	1-4GHz	43	70	39	129	83	-7
4	4-7GHz	43	70	40	130	85	-5
5	7-10GHz	43	70	42	132	80	-10

For most bands, the RF amplifier overloads first and the attenuation was placed at the amplifier inputs. (Output attenuation is to be preferred over input attenuation because the latter increases system noise figure. However, output attenuation below the detector overload point reduces dynamic range and thus should not be used as long as the system is not input-noise limited.)

For impulses, the CW specification Limit Detector Input was increased by $r = 20 \text{ dB}$ and by $20 \log_{10}$ of the RF bandwidth to obtain the Impulse Specification Limit Detector Input. This was then subtracted from the RF amplifier or detector overload point, whichever was lower, to obtain the Impulse Dynamic Range. Note that workable positive values now exist for Bands 1 and 2, and that these are relative to the new First Cut Specification Limits and not just to system sensitivity, as were the dynamic range figures in the second Quarterly Report.

The system CW sensitivity should now be checked. If the newly selected amplifiers have too high a noise figure, or if too much attenuation was used, the detected system noise might exceed the detected specification limit (threshold) antenna output and the system would not work.

The overall noise figure, F , for a system made up of several stages having individual noise figures, F_n , and individual gains, G_n , is given by

$$F = A_1 F_1 + \frac{A_2 (F_2 - 1)}{G_1} + \frac{A_3 (F_3 - 1)}{G_1 G_2} + \dots + \frac{A_n (F_n - 1)}{G_1 G_2 \dots G_{n-1}} \quad (10)$$

where A_n is the attenuation, if any, preceeding a particular amplifier stage. Note that attenuation following the last stage has no effect on noise figure.

The Band 1 antenna was assumed to have an overall noise figure of 16.4 dB including a 5 dB noise figure preamplifier. The newly selected preamplifier from Table 4 has a noise figure of 9 dB instead of 5 dB. Using the above equation, the noise figure of this antenna alone is:

$$\begin{aligned}
 F_1 &= \frac{G_1 F - A_2 F_2 + 1}{A_1 G_1} \\
 &= \frac{1(\log_{10}^{-1} 16.4/10) - 1(\log_{10}^{-1} 5/10) + 1}{(1)} \\
 &= 43.6 - 3.2 + 1 \\
 &= 41.4
 \end{aligned}$$

$$F_1 = 16.2 \text{ dB}$$

The overall Band 1 ($A_1 = A_2 = A_3 = A_4 = 1$) noise figure is

$$\begin{aligned}
 F &= F_1 + \frac{F_2 - 1}{G_1} + \frac{F_3 - 1}{G_1 G_2} + \frac{F_4 - 1}{G_1 G_2 G_3} \\
 &= 41.4 + \frac{7.94 - 1}{1} + \frac{7.94 - 1}{1(2.2)} + \frac{12.6 - 1}{1(2.2)^2} \\
 &= 53.9
 \end{aligned}$$

$$F = 17.3 \text{ dB}$$

The new noise figures for the various bands are shown in Table 6.

Table 6.
System Noise Figure

Band	A ₁	F ₁	G ₁	F ₂	G ₂	F ₃	G ₃	F ₄	G ₄	Overall Noise Figure	RF Noise Margin*	Possible CW** Sensitivity
1	0 (1)	16.2 (41.4)	0 (1)	9.0 (7.94)	7.0 (2.2)	9.0 (7.94)	7.0 (2.2)	11.0 (12.6)	7.0 (2.2)	17.3 dB	34.2 dB	6.9 dBμV
2	8.0 (6.3)	6.0 (3.98)	10.5 (3.35)	10.0 (10)	11.0 (3.55)	12.0 (15.8)	9.0 (2.82)			14.6	47.6	4.2
3	9.0 (7.9)	4.8 (3.0)	25.0 (17.8)							13.8	39.2	3.4
4	0 (1)	6.0 (3.98)	19.0 (8.91)							6.0	54.8	-4.4
5	3.0 (2.0)	5.5 (3.55)	22.0 (12.6)							8.5	49.8	-1.9

Note: Values shown are in decibel/(numerical) notation.

* At detector input = T_{ss}

** Given sufficient RF gain for input-noise-limited operation.

From Equation (9) of the second Quarterly Report, the peak narrowband input required for peak signal equal to peak noise in the output of the detector is:

$$V_{SI} = -0.4 + F + 5 \log_{10}(2B_O B_I - B_O^2) \text{ dBuV} \quad (11)$$

For Band 1:

$$\begin{aligned} V_{SI} &= -0.4 + 17.3 + 5 \log_{10}[2(50 \times 10^{-6})(100) - (50 \times 10^{-6})^2] \\ &= -0.4 + 17.3 - 10.0 \\ V_{SI} &= 6.9 \text{ dBuV} \end{aligned}$$

which is considerably more sensitivity than is needed to detect the 24 dBuV output of the antenna when operating in a field equal to the new Specification Limit. The sensitivities that could be possible with the noise figures calculated above are listed in Table 6. Most of the excess sensitivity has now been sacrificed in the interest of dynamic range by reducing RF gain to the point where an input equal to the possible sensitivity will not reach the detector threshold, but neither will system input noise. If sufficient gain were added to bring V_{SI} up to T_{SS} , there would be a RF noise safety margin for Band 1 of $24 - 6.9 = 17.1$ dB. Without the extra (excess) gain, the RF noise safety margin is doubled to 34.2 dB. The RF noise margins for the various bands are quite adequate, as shown in Table 6. (If more margin were needed, the attenuation could be partially apportioned between the various stages to lower the system noise figure somewhat without sacrificing dynamic range, or special amplifiers could be specified with exactly the right gains.)

The dynamic ranges shown in Table 5 are adequate for realistic operation of the system in Bands 1 and 2, i.e., up to 1 GHz. Above 1 GHz narrowband operation is satisfactory but truly broadband worst-case impulse signals will cause saturation before their presence is indicated on the output indicators. There are several possible approaches to the wideband interference measurement problem above 1 GHz;

- a. MIL-STD-461 has not previously been applied to broadband interference above 1 GHz. It could continue to be ignored. However, the Broadband Measurement System cannot at present differentiate between broadband and narrowband interference and the equipment saturation point will have to be standardized if consistent measurements are to be made with various realizations of the Broadband Measurement System.
- b. The RF bandwidth could be reduced above 1 GHz. A nominal 10 dB improvement is required which will need a reduction of $\log_{10}^{-1}(10/20)=3.16$ in impulse bandwidth. Going to 1 GHz bandwidths above 1 GHz would marginally cure the problem but would require 11 bands for complete coverage. (2 bands below 1 GHz and 9 bands above 1 GHz)
- c. The impulse/CW response ratio, r could be reduced from 20 dB to 10 dB. This would bring the new specification limits closer together than present MIL-STD-461 and cause concept acceptance difficulties.

For the present, it will be assumed that approach a. is viable. There is little likelihood that coherent interference occupying over a gigahertz of bandwidth at frequencies between 1 and 10 GHz will be significant. The system has marginally sufficient dynamic range to handle coherent broadband emissions occupying up to 1 GHz of bandwidth.

c) Broadband Measurement System, Second Cut

The preceeding sections outline some fairly significant changes in the hypothetical Broadband Measurement System since the initial design in the second Quarterly Report. Detector sensitivity has been improved through use of state-of-the-art detector diodes and the design concept has shifted from RF-input-noise-limited operation to detector-output-noise-limited operation in order to maximize dynamic range. As a result, a new RF amplifier lineup has been chosen with lower gain. These changes and more have been incorporated into the Second-Cut Block Diagram in Figure 3.

The antennas are unchanged. Single-pole, double throw (SPDT) solid-state RF switches have been added between the antennas and the RF amplifiers to connect a CW calibrator. The original amplifiers have been replaced with the amplifiers listed in Table 4. Full-wave biased detectors that will have to be custom built using state-of-the-art diodes replace the off-the-shelf coaxial detector assemblies previously used. A sample-and-hold circuit with analog-to-digital (A/D) converter and digital signal processing in a microcomputer replaces the earlier analog peak detector.

All of the blocks in Figure 3 appear to be readily realizable. The CW calibrator can be a pair of Avantek VTO-8240 voltage-tuned oscillators hetrodyned together in the 2.2 to 3.7 GHz range to produce signals in each band under frequency control of the microcomputer. A specific manufacturer has not been identified for the 14 kHz to 100 MHz RF switch but the requirements appear to be suited to field-effect-transistor (FET) switch technology. The video filters present some problems in that a filter having a DC to 3 GHz input and a low-pass output of a few hertz is unusual. The main requirement is that the filter must present a well-matched 50-ohm input to all frequencies from DC to 3 GHz without spurious responses. The filter sharpness is not critical as long as the impulse bandwidth is controlled. The filter should be realizable using microwave-type low-pass components to avoid parasitic reactances.

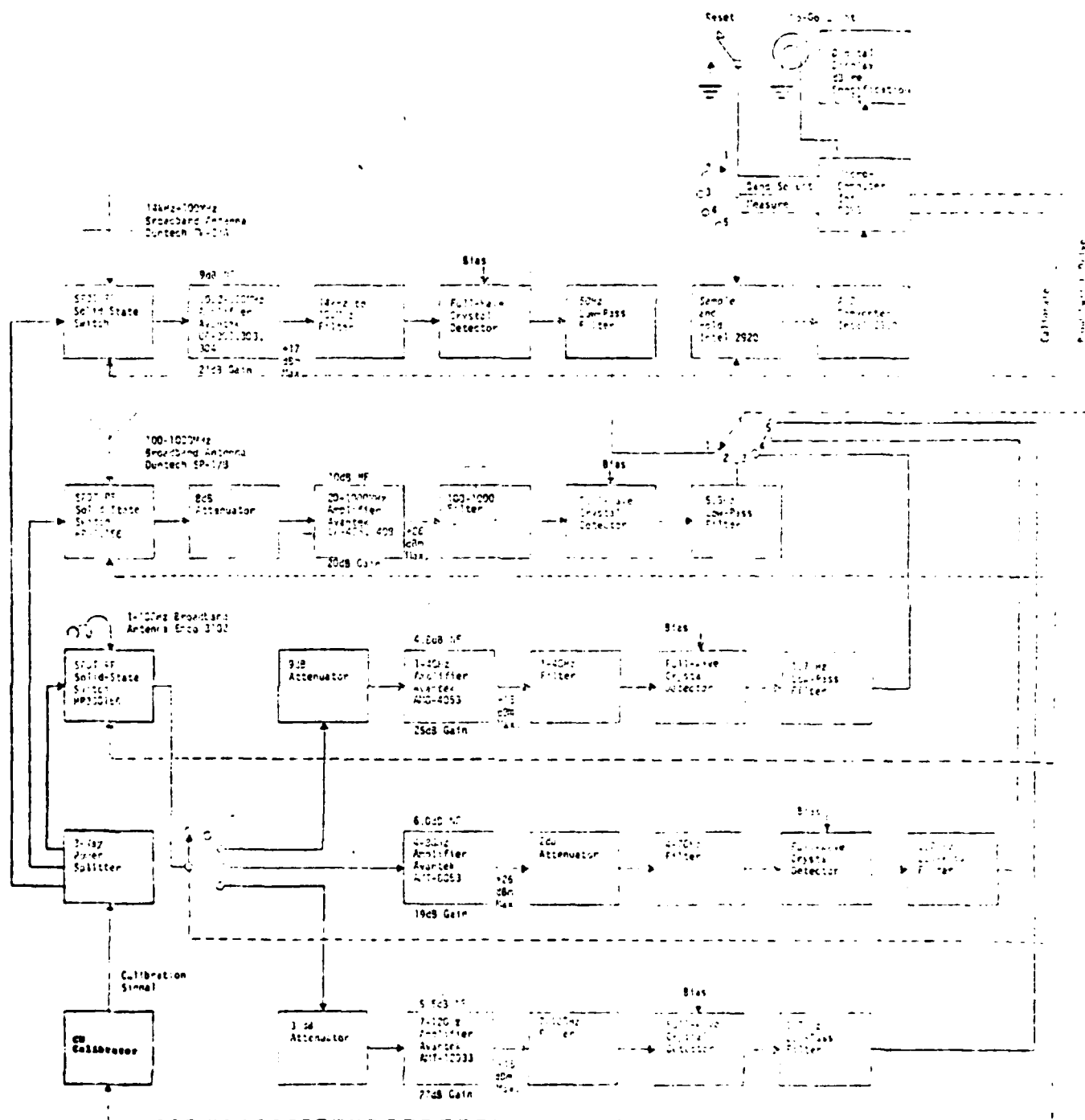


FIGURE 3. BROADBAND MEASUREMENT SYSTEM BLOCK DIAGRAM, SECOND CUT

Automatic calibration would occur every few seconds. The rate should be low enough that the ratio of measurement time to calibration time is large. The microcomputer would first switch the RF inputs to the calibrator and make system noise measurements on every band. CW signals at levels corresponding to the new specification limits would then be sent to each of the inputs and the output from each band measured and stored sequentially. Comparison of the stored calibration levels ($S+N$) with the noise measurements (N) would be used as an indication of proper system operation since $S+N$ should be greater than N alone. The switches would then reconnect the antennas. Incoming signals would then be compared with the stored calibration levels, the differences in dB computed and displayed, and the no-go light turned on if the levels exceed the limits.

2) Experimental Verification

Several curves were obtained experimentally using an unbiased Hewlett-Packard 420B Coaxial Crystal Detector to verify the equations developed in the second Quarterly Report. The detector uses a negative-polarity point-contact diode. Although frequency response is rated as ± 3.5 dB from 0.01 to 12.4 GHz, the only limit on low frequency response is RF leakage through the video connector and the experiments were successfully carried out at frequencies below 1 MHz using external filters. Voltage sensitivity (γ) is rated as 0.1 mV/LW.

a) Detector Conversion Response

The crystal detector was set up with adjustable filters initially set to provide a 100 kHz to 1 MHz pre-detection filter and a DC to 100 kHz post detection filter as shown in Figure 4. The input was then driven in turn from a CW generator, a noise source and an impulse generator. Amplifiers were used as necessary to bring the drive levels up into the operating range of the crystal detector.

Curves obtained by varying the peak input level and measuring the peak output level are shown in Figure 5. These curves have been termed Detector Conversion Response curves because the presence of the detector is necessary to convert energy input above 100 kHz to energy output below 100 kHz. Note that CW, which is unaffected by bandwidth ratios, has the highest output. Noise, whose power is affected by the bandwidth ratio, has the next highest output. Impulses, for which both power and peak voltage are affected by the bandwidth ratio, has the lowest output.

Using the equations developed in the second Quarterly Report for the transfer of energy through a square-law detector,

$$\frac{V_{IO}}{V_{SO}} = \frac{b(\sqrt{2}IB_I)^2}{V_{SI}^2} = b \left[\frac{V_{II}}{V_{SI}} \right]^2 \quad (12)$$

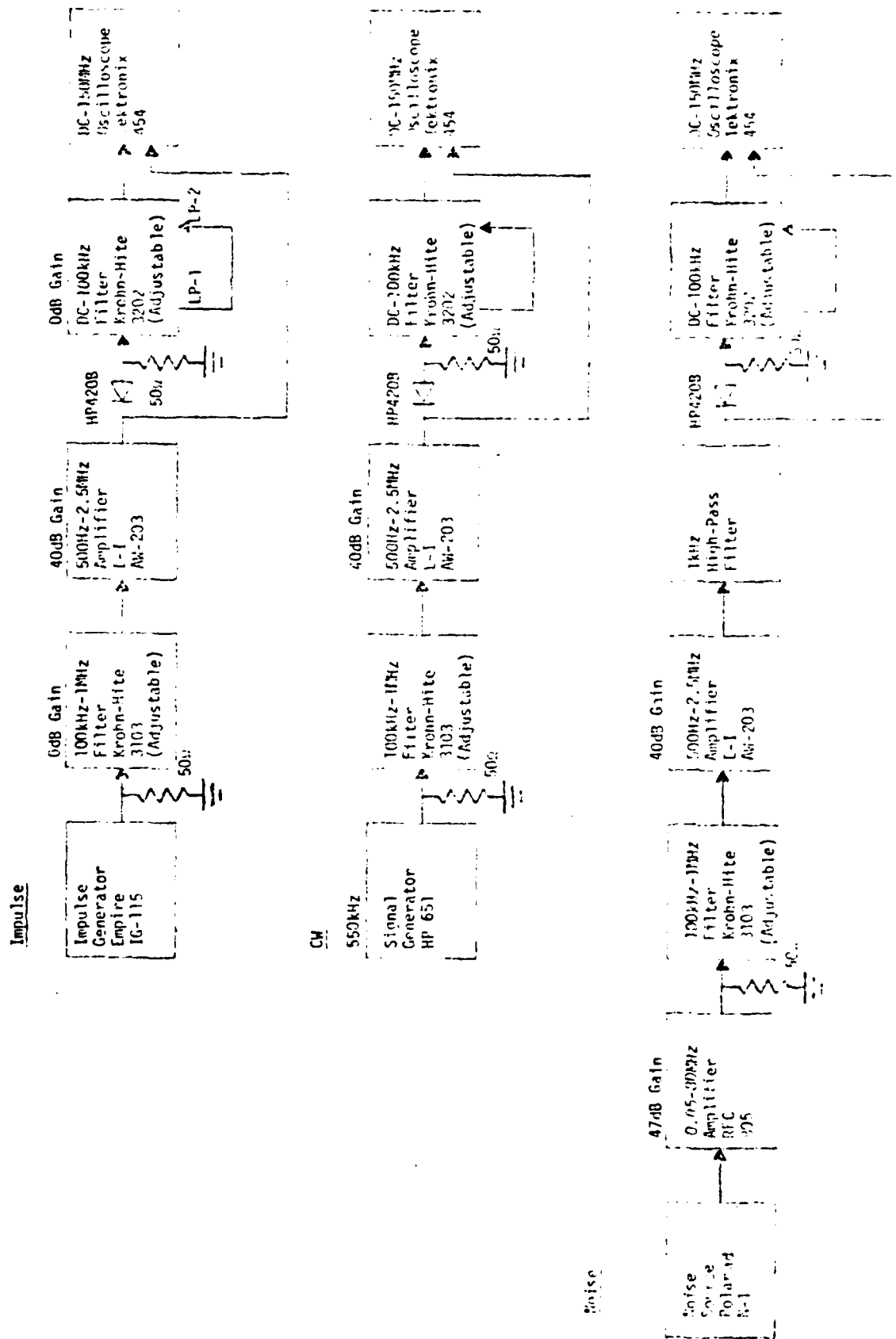


FIGURE 4. DETECTOR CONVERSION RESPONSE MEASUREMENT BLOCK DIAGRAMS

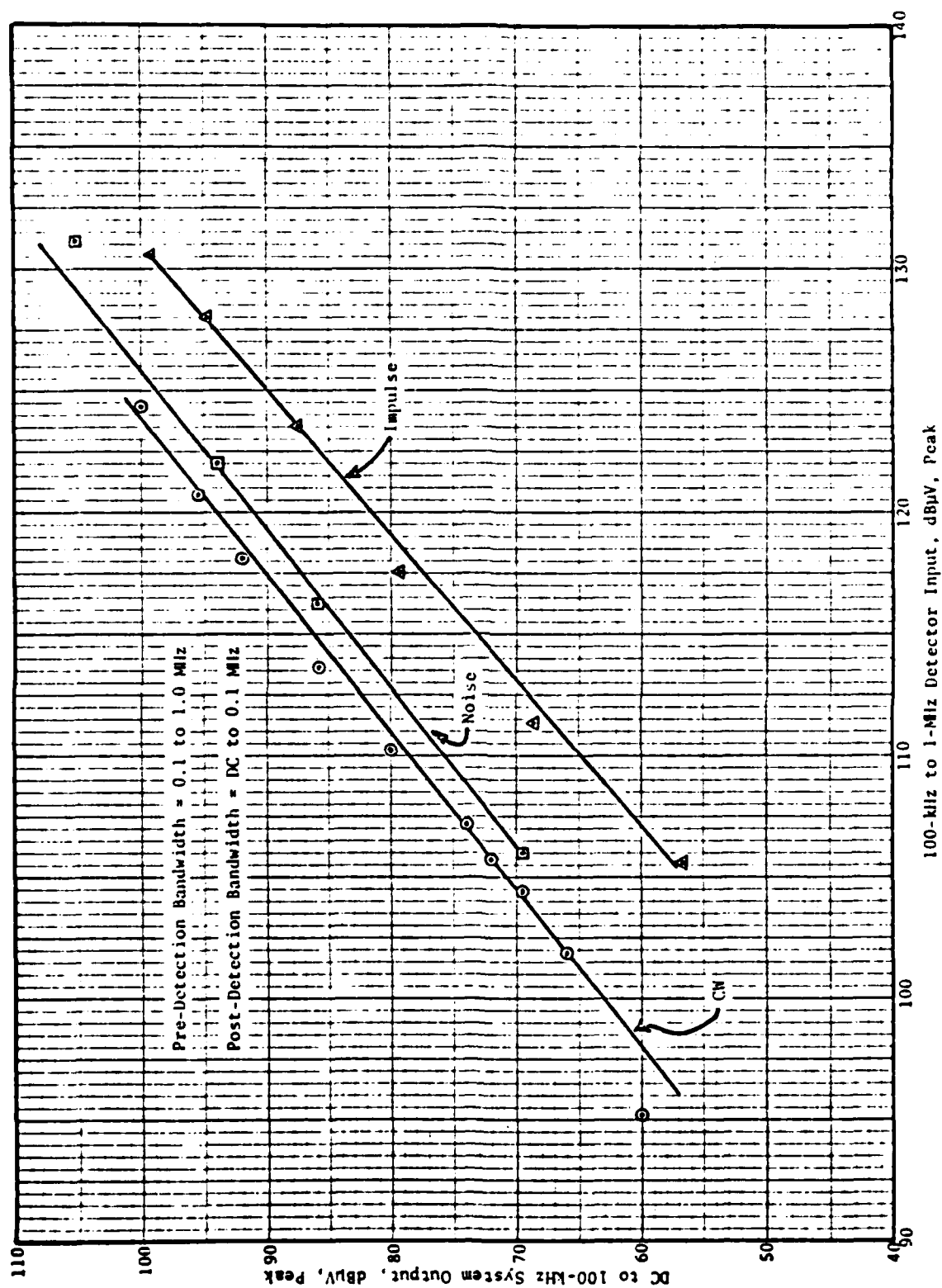


Figure 5. Detector Conversion Response.

where V_{IO} is the peak impulse voltage output, V_{SO} is the peak CW signal voltage output, I is the RMS impulse voltage input per unit bandwidth, B_I is the input bandwidth, V_{SI} is the peak CW signal voltage input, V_{II} is the peak impulse voltage input and

$$b = \frac{2B_0B_I - B_0^2}{B_I^2} \quad (13)$$

where B_0 is the output bandwidth.

Equation (12) can be generalized to an nth-law detector by replacing the exponent to obtain:

$$\frac{V_{IO}}{V_{SO}} = b \left[\frac{V_{II}}{V_{SI}} \right]^n \quad (14)$$

Replacing the impulse with noise, Equation (14) becomes:

$$\frac{V_{NO}}{V_{SO}} = \sqrt{b} \left[\frac{V_{NI}}{V_{SI}} \right]^n \quad (15)$$

The above equations are purposely kept in the form of ratios so that many of the system constants, such as the detector voltage sensitivity, will cancel and not require evaluation. Reasoning along the same line, use of these ratios in the hypothetical Broadband Measurement System reduces the effects of hardware variables. The equations assume that peak voltage input translates simply to peak voltage output which, as will be seen later, causes errors in constants which, while significant,

can be removed by calibration. Converting to decibel relationships, Equations (14) and (15) become:

$$20 \log_{10} \frac{V_{IO}}{V_{SO}} = 20 \log_{10} b + n (V_{II} - V_{SI}) \text{ dB} \quad (16)$$

and

$$20 \log_{10} \frac{V_{NO}}{V_{SO}} = 10 \log_{10} b + n(V_{NI} - V_{SI}) \text{ dB} \quad (17)$$

where the voltage inputs are in peak dB μ V.

For the experimental system used to obtain the data for Figure 5, $B_O = 0.1$ MHz and $B_I = 0.9$ MHz (nominal 3 dB bandwidths because more exact impulse bandwidths are not available) giving the following value for the bandwidth ratio from Equation (13):

$$b = \frac{2(0.1)(0.9) - (0.1)^2}{(0.9)^2}$$

$$= 0.210$$

$$10 \log_{10} b = -6.8 \text{ dB}$$

$$20 \log_{10} b = -13.6 \text{ dB}$$

The detector response law, n , can be obtained from the slope of the curves in Figure 5 as 1.55. Substituting these values into Equation (16) gives the following expression for the impulse-to-CW response ratio:

$$20 \log_{10} \frac{V_{IO}}{V_{SO}} = -13.6 + 1.55(V_{II} - V_{SI}) \text{ dB} \quad (18)$$

For equal inputs, Equation (18) predicts an impulse-to-CW output ratio of -13.6 dB. This compares favorably with the values of -12 to -14 dB obtained from the experimental data plotted in Figure 5 by scaling the vertical separation between the impulse and CW response curves. Values for several calculated and measured ratios are compared in Table 7. Good correlation between calculated and measured values are shown for the 1.55-law detector. The square-law assumption, shown for comparison, entails large errors.

Substituting values into Equation (17) provides the following expression for the noise-to-CW response ratio:

$$20 \log_{10} \frac{V_{NO}}{V_{SO}} = -6.8 + 1.55(V_{NI} - V_{SI}) \text{dB} \quad (19)$$

For equal inputs, Equation (19) predicts an output ratio of -6.8 dB which, when compared with the experimental value of -2.7 dB shows a rather significant 4.1 dB difference. The error is consistent over a range of input ratios as can be seen in Table 8, indicating that the detector response law is correct but that the constant is off. That these simplistic general equations predict results that are confirmed as closely as they are by measurements on an arbitrary experimental system is a tribute to the power of ratios.

For more exact results, the equations require some modification to apply to the experimental setup. Referring to Figure 4, the detector was operated into a 50-ohm video load. It was verified experimentally that at this low load resistance, the output of the detector was a half-wave rectified replica of the input waveform distorted only by the detector response law for all frequencies of interest here (i.e., no peak storage effects occurred in the output bypass capacitor.) The detector output, when passed through the DC to 100 kHz output low-pass filter, thus contains the average value as a DC component with whatever detected AC components will pass through the filter riding on it (i.e., the detector operates as an average detector.)

Table 7.

Impulse/CW Detection Conversion Response

$\frac{V_{II} - V_{SI}}{V_{IO}/V_{SO}}$	Measured $\frac{V_{IO}}{V_{SO}}$	Calculated $\frac{V_{IO}}{V_{SO}}$		1.55 Law	Error
		Square-Law	Error		
0 dB	-12 dB	-13.6 dB	-1.6 dB	-13.6 dB	-1.6 dB
8	0	2.4	2.4	- 1.2	-1.2
16	12	18.4	6.4	11.2	-0.8
20	19	26.4	7.4	17.4	-1.6
24	25	34.4	9.4	23.6	-1.4

Table 8.

Noise/CW Detector Conversion Response

$\frac{V_{NI}}{V_{SI}}$	Measured $\frac{V_{NO}}{V_{SO}}$	Calculated*	
		$\frac{V_{NO}}{V_{SO}}$	Error
0 dB	- 2.7 dB	- 6.8 dB	- 4.1 dB
8	9.6	5.6	- 4.0
16	22.0	18.0	- 4.0
20	28.0	24.2	- 3.8
24	34.4	30.4	- 4.0

* For 1.55-Law Detector Using Equation (19)

(1) CW Detailed Analysis

For a CW input of $V_{SI} = A \sin \omega t$, the output of a square-law detector before filtering is:

$$\begin{aligned} V_{SO} &= CV_{SI}^2 \\ &= CA^2 \sin^2 \omega t \\ &= CA^2 \sin^2 \frac{2\pi t}{T_s} \end{aligned} \quad (20)$$

where T_s is the period and A is the peak voltage of the input sinewave, and C is a detector sensitivity constant. The area under the half-wave rectified detector output when plotted against time, t , will be:

$$\begin{aligned} \text{Area} &= \int_0^{T_s/2} A^2 \sin^2 \left(\frac{2\pi t}{T_s} \right) dt \\ &= A^2 \left[(T_s/4) - (\sin 2\pi)/(8\pi/T_s) \right] \\ &\quad - 0 + (\sin 0)/(8\pi/T_s) \\ &= \frac{T_s A^2}{4} \end{aligned} \quad (21)$$

The area divided by T_s is the average, or DC, value of V_{SO} . Thus:

$$\begin{aligned} V_{SO} T_s &= \frac{CT_s A^2}{4} \\ V_{SO} &= \frac{CA^2}{4} \end{aligned} \quad (22)$$

and the CW output from the experimental detector after filtering should be one-quarter of the peak input when adjusted for detector sensitivity.

Thus, for an nth-law detector:

$$V_{SO} = 0.25C V_{SI}^n \quad (23)$$

Use of a detector response law other than 2 (i.e., square-law) will have an effect on the average value by changing the exponents used in Equation (20) from 2 to n, but this makes integration difficult. The effect should be small since V_{SO} only changes from $A^2/4$ to A/π if the exponents are taken all the way to unity, representing a maximum possible change in V_{SO} of -2.1 dB.

(2) Impulse Detailed Analysis

The impulse spectrum consists of a series of equal amplitude sine waves (Fourier Components) spaced at the impulse repetition frequency across the input bandwidth. Thus for the experimental setup which used an impulse generator synchronized to the power line, sine wave components were spaced every 60 Hz over the input bandwidth from 0.1 to 1.0 MHz. If it is assumed that each of these sine-wave components is half-wave rectified to produce average values (which add algebraically to produce the instantaneous impulse output) in the same manner as for CW, then it follows that the peak impulse input voltage will be related to the peak impulse output voltage by the same ratio as peak CW input is related to peak CW output. (For CW, the peak and average output values are synonymous with the DC component after filtering.) The experimental data bear out this assumption. Thus:

$$V_{IO} = 0.25C_b V_{II}^n \quad (24)$$

(3) Noise Detailed Analysis

For noise, the detector averages the output much the same as for CW except that some detected AC noise appears in the output along with the DC component. When the output bandwidth, B_O , is small in comparison with the input bandwidth, B_I , as it was in the experimental setup, the AC component will be small in comparison to the DC component in the video filter output, and only the DC component will remain as the output bandwidth approaches zero.

Comparison of peak values of noise observed on the oscilloscope with RMS values measured on a true-RMS voltmeter during the experimental measurements indicated that a peak-to-RMS ratio (peak factor) of 3 would include nearly all of the observed peaks both before and after the detector. The noise distribution before the detector would be expected to be Gaussian, for which a peak factor of 3 has a probability of being exceeded 0.1 percent of the time.⁴ The noise distribution after a linear detector would be expected to be Rayleigh, for which a peak factor of 3 has a probability of being exceeded 0.01 percent of the time (See Section 3b of the second Quarterly Report.) The measurement technique should measure peak amplitudes corresponding to constant probability with the result that a lower peak factor would be expected after the detector than before. The apparent discrepancy is the result of the greater than unity detector response law (1.55 in the experimental setup) which tends to increase the peak factor in the output over that which would exist if the response law were unity.

4. Bennett: "Electrical Noise", McGraw-Hill, 1960, p. 44.

From Section 3b of the second Quarterly Report, the noise power in the detector output is:

$$P_{NO} = b(CNB_I)^2 \quad (25)$$

where b is given by Equation (13) and N is the noise power per unit bandwidth at the input. Converting from noise power to noise voltage in a system with the same impedances as used previously for CW and impulses, the peak noise output voltage is:

$$V_{NO} = C \sqrt{b} V_{NI}^2 \quad (26)$$

where V_{NI} is the peak noise input voltage. Generalizing to an n th-law detector. Equation (26) becomes:

$$V_{NO} = C \sqrt{b} V_{NI}^n \quad (27)$$

where n is the detector response law.

Assuming a linear envelope detector and that V_{NO} has a Rayleigh distribution, the average, or DC, component in the detector output is:¹

$$V_{NO/DC} = \sqrt{\pi/2} \sigma \quad (28)$$

where σ is the RMS value of the input noise voltage. The RMS value of V_{NO} for an envelope detector before filtering is $\sqrt{2}\sigma$, which includes both DC and AC components. The RMS AC component

before filtering can be obtained by subtracting the square of the DC component (proportional to DC power) from the square of the total (proportional to total power) and taking the square root as $\sqrt{2-(\pi/2)}\sigma$. The effect of filtering can then be obtained by multiplying by the square root of the bandwidth ratio, \sqrt{B} , and the measured output peak factor, F_{PO} , to obtain:

$$V_{NO/AC} = F_{PO} \sqrt{B[2-(\pi/2)]} \sigma \quad (29)$$

However, the experimental detector is not a linear envelope detector, but is instead an nth-law average detector. Taking the envelope versus average detector problem first, an envelope detector assumes peak detection with storage between peaks so that the envelope has a higher RMS value than the original wave. This is reflected in the usual notation for the Rayleigh distribution by the RMS value of the distribution being $\sqrt{2}$ times the RMS value of the input waveform, σ . The peak-to-RMS ratio for a sine wave is also $\sqrt{2}$. For an average detector, the output is still proportional to the envelope of the input waveform, but is attenuated to reflect the average value instead of the peak value. Assuming that noise behaves in the detector much like a sine wave of equal RMS value, the derivation of Equation (23) would be expected to apply with the result that:

$$\sigma = 0.25C \left[\frac{\sqrt{2} V_{NI}}{F_{PI}} \right]^n \quad (30)$$

where V_{NI}/F_{PI} is the RMS value of the input noise which, when multiplied by $\sqrt{2}$, results in the peak value of the equivalent sine wave.

The peak noise voltage at the detector output after filtering is the algebraic sum of the DC and peak AC components:

$$V_{NO} = V_{NO/DC} + V_{NO/AC}$$

$$= \sqrt{\pi/2} \sigma + F_{PO} \sqrt{b[2-(\pi/2)]} \sigma$$

$$= 0.25C \left[\frac{\sqrt{2V_{NI}}}{F_{PI}} \right]^n (\sqrt{\pi/2} + F_{PO} \sqrt{b[2-(\pi/2)]}) \quad (31)$$

Equation (31), by making use of the concept of an equivalent sine wave, avoids the messy problem of modifying the Rayleigh distribution to take into account the actual detector characteristics. Bracewell⁵ states that the output envelope from a square-law detector with Gaussian input has a truncated exponential distribution, which is a considerable change from Rayleigh. The envelope from an nth-power law detector would supposedly have somewhere between a Rayleigh and a truncated exponential distribution. In spite of the approximations involved, the equations in this Section agree well with the limited experimental data available.

5. R. Bracewell "The Fourier Transform and Its Applications" McGraw-Hill, 1965, p. 337.

(4) Revised Detector Conversion Response Predictions

The significance of the 4.1 dB difference between the values of detector conversion response calculated using Equation (15) and the experimentally measured values is now apparent. Equation (15) ignores the DC component which results when noise, or any other signal with significant energy density over time, is rectified. The revised expression for the noise-to-CW response ratio is obtained from Equations (23) and 31) as:

$$\frac{V_{NO}}{V_{SO}} = \left[\frac{\sqrt{2} V_{NI}}{F_{PI} V_{SI}} \right]^n (\sqrt{\pi/2} + F_{PO} \sqrt{2 - (\pi/2)}) \quad (32)$$

where the two terms in parenthesis are the DC and AC output noise components, respectively. Converting to decibel relationships:

$$\begin{aligned} 20 \log_{10} \frac{V_{NO}}{V_{SO}} &= 20 \log_{10} (\sqrt{\pi/2} + F_{PO} \sqrt{2 - (\pi/2)}) \\ &\quad + n (20 \log_{10} \sqrt{2} - 20 \log_{10} V_{NI} - 20 \log_{10} V_{SI} - 20 \log_{10} F_{PI}) \\ \text{from which} \\ 20 \log_{10} \frac{V_{NO}}{V_{SO}} &= 20 \log_{10} (1.253 + F_{PO} \sqrt{.4295}) \\ &\quad + n (3.0 + V_{NI} - V_{SI} - 20 \log_{10} F_{PI}) \end{aligned} \quad (33)$$

where V_{NI} and V_{SI} are in peak dBuV.

For the experimental setup:

$$\begin{aligned} 20 \log_{10} \frac{V_{NO}}{V_{SO}} &= 20 \log_{10} (1.253 + 3 \sqrt{.429} (0.210)) \\ &\quad + 1.55 (3.0 - 20 \log_{10} 3 + V_{NI} - V_{SI}) \\ &= 20 \log_{10} (1.253 + 0.900) + 1.55 (3.0 - 9.5 + V_{NI} - V_{SI}) \\ &= 6.7 + 4.6 - 14.7 + 1.55 (V_{NI} - V_{SI}) \\ &= -3.4 + 1.55 (V_{NI} - V_{SI}) \text{ dB} \end{aligned} \quad (34)$$

For equal peak noise and peak CW input, Equation (34) predicts an output response ratio of -3.4 dB which compares favorably with the measured value of -2.7 dB. A comparison of several measured and calculated values is shown in Table 9. The agreement is now quite close throughout the range.

The ratio of DC-to-AC noise output components predicted by Equation (31) is also in reasonable agreement with experimental values. This ratio can be evaluated using values from the first term of Equation (34) as $1.253/0.900 = 1.392$. During the measurements, a typical composite peak noise output reading of 0.18 volts was noted to drop to 0.10 volt DC when the output low-pass filter cutoff frequency was reduced from 100 kHz to 20 Hz. This indicates that, of the 0.18 volts composite peak output, 0.10 volt was DC and 0.08 volt was peak AC, for a ratio of $0.10/0.08 = 1.3$. Similar ratios were obtained at other output levels.

The impulse-to-CW response ratio remains unchanged by the detailed analysis. However, the same problem exists as existed for the noise-to-CW response ratio in that the DC component is ignored by Equation (3). This will not cause a problem as long as the impulse repetition rates are small in comparison with the output bandwidth so that the effect of one impulse has died out before another occurs. Faster impulse repetition rates and smaller output bandwidths will eventually entail generation of a significant DC component. The additional output will increase the sensitivity to repetitive broadband emissions and have to be recognized as equivalent to a reduction in specification limits for repetitive as opposed to singular broadband events when writing the Broadband Measurement Specification for use with the Broadband Measurements System. This can best be handled by having the broadband limit apply to single impulse events and the narrow-band limit apply to CW with the understanding that everything else will fall into place.

Table 9.
Revised Noise/CW Detector Conversion Response

$\frac{V_{NI}}{V_{SI}}$	Measured $\frac{V_{NO}}{V_{SO}}$	Calculated* $\frac{V_{NO}}{V_{SO}}$	Error
0 db	- 2.7 dB	- 3.4 dB	- 0.7 dB
8	9.6	9.0	- 0.6
16	22.0	21.4	- 0.6
20	28.0	27.6	- 0.4
24	34.4	33.8	- 0.6

* For 1.55-Law Detector using Equation (34).

b) Bandwidth Factors

Referring to the experimental measurement system block diagram in Figure 4, both the pre-detection and post-detection filters were variable. Measurements were made as the filters were varied with both noise and impulses as inputs. While measurements were not actually made of the effect of bandwidth on CW because the data would be trivial, CW was used as a calibrating signal and to obtain frequency response curves.

Throughout the experimental data, the cutoff frequencies recorded are the settings of the Krohn-Hite filter dials with the filters set for "flat response" as opposed to "RC response", and are nominal 3 dB values. The pre-detection filter had rated high-pass and low-pass slopes of 24 dB/octave. The post-detection filter had two low-pass sections rated 24 dB/octave synchronously tuned to give an overall slope of 48 dB/octave. The impulse bandwidths were not measured and, in the calculations, are assumed to be the same as the nominal bandwidths. Impulse bandwidths are normally somewhat wider than 3 dB bandwidths, but since bandwidths are used in ratio in most of the calculations, the error should be within experimental accuracy.

(1) Effect of Bandwidth on Noise

A plot of the effects of varying bandwidths on white noise is shown in Figure 6. The pre-detection bandwidth was left fixed at 900 kHz while the post-detection bandwidth was varied from 100 kHz down to 20 Hz to obtain the Post-Detection Filter curves on the left. The post-detection low-pass filter was set to 100 kHz, and the pre-detection low-pass filter varied from 1.0 MHz down to 150 kHz to obtain the Pre-Detection Filter curves on the right.

Two curves were obtained as the result of varying the post-detection low-pass filter bandwidth. The first was measured on a DC-coupled oscilloscope and represents the peak value of the composite AC and DC components. The second represents the peak AC component alone, and was measured with an AC-responding true-RMS voltmeter. The RMS readings were converted to peak

before plotting by multiplying by the experimentally determined output peak factor, F_{p0} , of 3. The DC component alone was a constant 100 dB μ V (or 0.1 volt) independent of bandwidth.

The ratio of peak AC to DC shown by the Post-Detection Filter curves is in good agreement with Equation (21) as detailed in the preceeding subsection. Perhaps even more important, the slope of the Peak Value of the AC Noise curve is almost exactly 10 dB/decade, which confirms that the peak AC component varies as \sqrt{B} in agreement with Equation (21) and the derivations in the previous Quarterly Report which led up to it.

The slope of the Pre-Detection Filter curve for peak combined noise and DC is also 10 dB/decade, but it is the DC component that is varying rather than the AC component that had varied in the Post-Detection Filter curves. The peak AC component stay constant until the low-pass pre-detection filter stopband overlaps the high-pass pre-detection filter stopband. This also is in agreement with the \sqrt{B} term in Equation (31) which requires that the output AC component decrease with increasing input bandwidth by the same amount that the input noise voltage increases resulting in no net change in the output AC component. The input noise voltage changes with bandwidth at the rate of 10 dB/decade because the curves were run with constant input noise power per unit bandwidth. This is reflected directly in the predominant DC component which is unaffected by output bandwidth.

The RF bandpass characteristic of the pre-detection amplifiers and filter combined is plotted in Figure 6 for reference. The characteristic reflects an overshoot in the amplifier gain which occurs just before the gain falls off rapidly above 2 MHz.

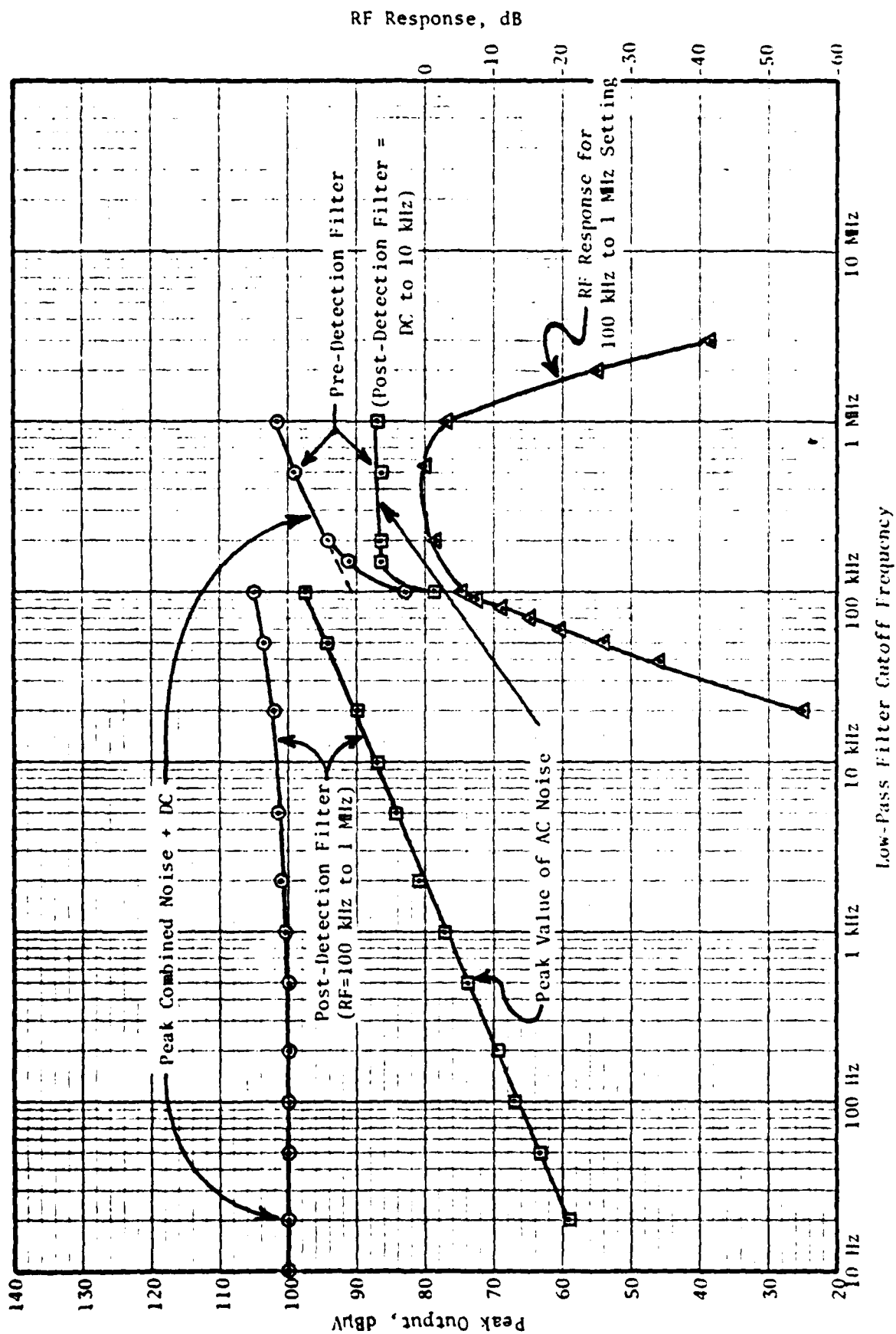


Figure 6. Effect of Low-Pass Filtering on Noise Output, RF High-Pass = 100 kHz.

(2) Effect of Bandwidth on Impulses

The effect of bandwidth on impulses in the experimental measurement setup is shown in Figure 7. A set of post-detection filter curves was obtained by setting the pre-detection filter for a 0.1 to 1.0 MHz passband and varying the post-detection low-pass cutoff frequency from 2 MHz (the maximum capability of the filter) down to 1 kHz (where the signal disappeared into noise).

Measurements of post-detection-bandwidth effects were made both with the detector in the circuit and with the detector removed, leaving the rest of the system unchanged. The curve obtained without the detector shows direct feedthrough of impulses changing level at the expected rate of 20 dB/decade in the region between 0.2 and 1.0 MHz where the passbands of both filters overlap. The rolloff in the pre-detection filter just begins to show up between 1 and 2 MHz. Below 0.2 MHz, the rolloff due to the pre-detection filter is quite pronounced and the signal disappears into noise at about 50 kHz.

Adding the detector reduces the output level in the feedthrough region between 0.1 and 1.0 MHz because of the loss in the detector. However, there is now output below 0.1 MHz which did not exist without the detector. This graphically illustrates the concept of detector conversion response in which a spectrum centered at some high frequency is converted to a spectrum centered around zero frequency. Interestingly, the noise was so reduced by the detector that the output with detector was measureable into noise. Also interestingly, there is no discontinuity in the output with detector as the output filter passes out of the feedthrough region. The former illustrates the signal-to-noise (S/N) improvement in a high-law detector (an 8 dB S/N output for T_{ss} in a square-law detector, for example, requires an input S/N of only 4 dB.) The latter implies that direct feedthrough will not interfere with the measurement of detected impulses.

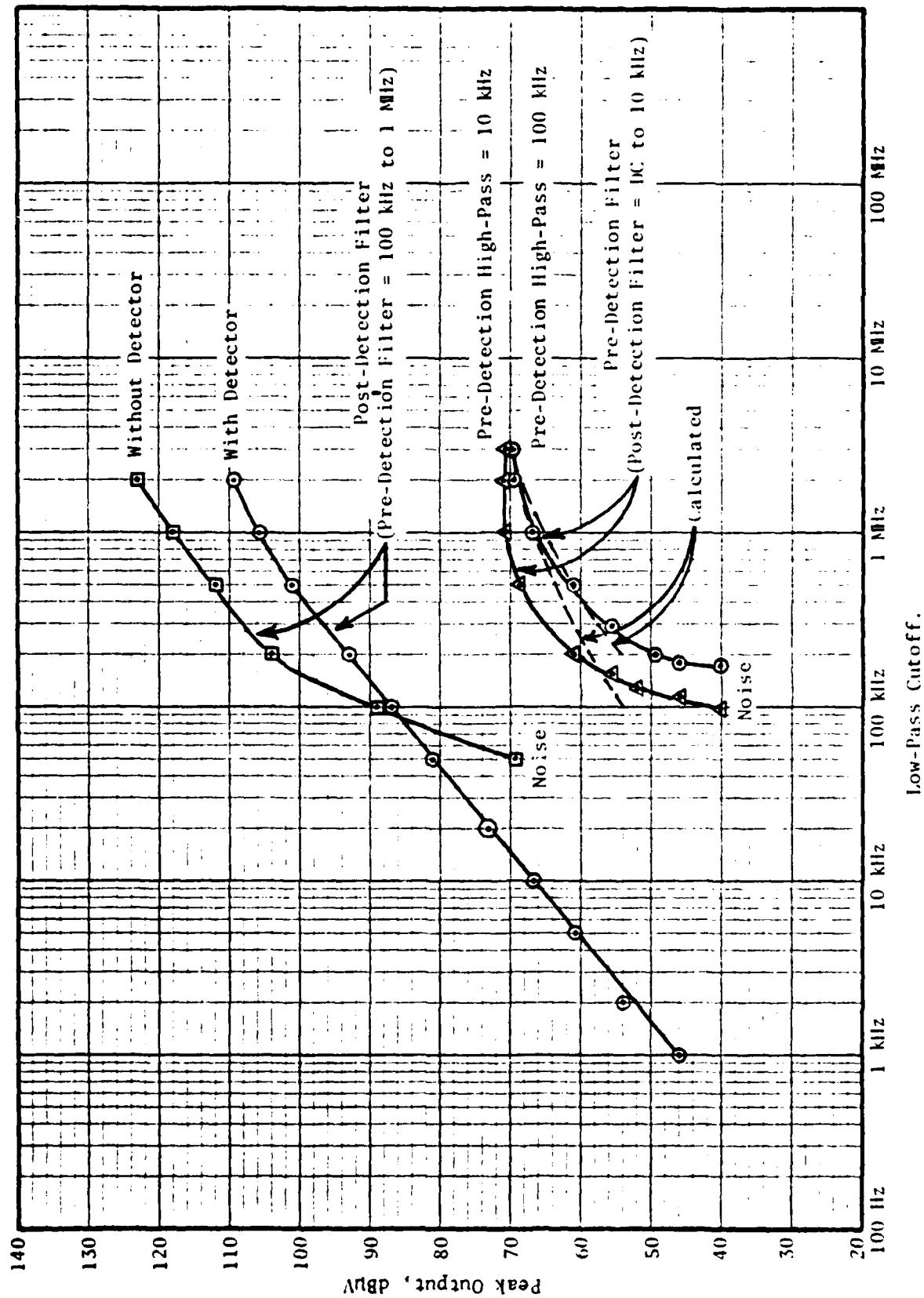


Figure 7. Effect of Low-Pass Filter Cutoff Frequency on Impulse Output.
RF High-Pass = 100 kHz, Input = 120.0 dBuV/MHz.

The slope of the detected output level versus the post-detection filter bandwidth is exactly 20 dB/decade. This agrees nicely with Equation (13) which requires that the impulse response vary directly with the bandwidth ratio, b .

The remaining curves in Figure 7, illustrating pre-detection filter effects, caused some consternation when they were first plotted. These curves were obtained by leaving the post-detection bandwidth fixed at DC to 10 kHz and varying the pre-detection bandwidth. The first curve plotted left the high-pass cutoff fixed at 100 kHz and varied the low-pass cutoff from 3 MHz down to 100 kHz. The response started dropping off rapidly somewhat before the lower band edge was reached, but then perhaps the filter wasn't too accurate. Then the high-pass cutoff was moved down to 10 kHz and a second curve plotted. This time there was no question of filter accuracy. The response fell off almost as fast as before and had dropped into noise long before the band edge was even approached. Also, the flatness at the upper ends of the curves was suggestive of saturation, but care had been exercised to avoid saturation.

The effects noted are a surprisingly illuminating confirmation of Equation (24). This equation when re-written in decibel relationships, without the unimportant (here) detector constant 0.25C, is:

$$\begin{aligned} V_{IO} &= 20 \log_{10} b + 1.55 V_{II} \\ &= 20 \log_{10} \left[\frac{2B_I B_O - B_I^2}{B_O^2} \right] + 1.55 V_{II} \end{aligned} \quad (35)$$

where V_{II} is the peak impulse input voltage in dBV. Taking as an arbitrary input level an impulse signal, I , of 1.0 V/MHz in an input band from 0.10 to 3.00 MHz for which $V_{II} = IF_I = 1.0(3.00-0.10) = 2.90$ volt, a reference output for comparing calculated and measured data is:

$$\begin{aligned}
V_{IO} &= 20 \log_{10} \left[\frac{2(0.01)(2.90) - 0.0001}{2.90^2} \right] \\
&\quad + 1.55 (20 \log_{10} 2.90) \\
&= 20 \log_{10} (6.88 \times 10^{-3}) + 1.55 (9.2) \\
&= -43.2 + 14.3 \\
&= -28.9 \text{ dBV}
\end{aligned}$$

Values of V_{IO} with a constant arbitrary 1.0 V/MHz input impulse are shown in Table 10 for several input low-pass filter cutoff frequencies pertinent to Figure 7. Using the 3 MHz low-pass cutoff values as references, the change in V_{IO} as the low pass cutoff frequency is reduced were then tabulated for comparison with the corresponding measured changes and plotted as dashed lines in Figure 7.

There is excellent similarity between the calculated and measured Pre-Detection Filter curves for the 100 kHz high-pass condition. The differences are somewhat greater for the 10 kHz high-pass condition, but the important characteristic of increasing slope as bandwidth decreases is there. The measured curves are somewhat flattened at their upper ends by the Electro-International AW-203 amplifier frequency response which peaks by a couple of dB around 1 MHz and then is down by 3 dB at 2.5 MHz. At the lower ends, the detector response law may be increasing toward square-law, or even higher as diode conduction ceases. The lower-end levels are close to noise and below those used in Figure 5 to establish the 1.55-law for the experimental detector.

Table 10.
Effects of Pre-Detection Filtering on Impulse Response

Pre-Detection High-Pass Filter Cutoff Frequency = 100 kHz

Pre-Detection Filter			b	V_{II}^*	1.55		Change In V_{IO} RE: 3 MHz	
Low-Pass Cutoff	High-Pass Cutoff	Bandwidth B_I			V_{II}	V_{IO}	Calculated	Measured
3.0 MHz	0.10 MHz	2.90 MHz	-43.2dB	9.2dBV	14.3dBV	-28.9dBV	0 dB	0 dB
2.00	0.10	1.90	-39.6	5.6	8.7	-30.9	- 2.0	0
1.00	0.10	0.90	-33.1	- 0.9	- 1.4	-34.5	- 5.5	- 3
0.50	0.10	0.40	-26.1	- 8.0	-12.4	-38.5	- 9.6	- 9
0.20	0.10	0.10	-14.4	-20.0	-31.0	-45.4	-16.5	-20

Pre-Detection High-Pass Filter Cutoff Frequency = 10 kHz

Pre-Detection Filter			b	V_{II}^*	1.55		Change In V_{IO} RE: 3 MHz	
Low-Pass Cutoff	High-Pass Cutoff	Bandwidth B_I			V_{II}	V_{IO}	Calculated	Measured
3.00 MHz	0.01	2.99 MHz	-43.5dB	9.5dBV	14.7dBV	-28.8dBV	0 dB	0 dB
2.00	0.01	1.99	-40.0	6.0	9.3	-30.7	- 1.9	0
1.00	0.01	0.99	-33.9	- 0.1	- 0.2	-34.1	- 5.3	0
0.50	0.01	0.49	-27.9	- 6.2	- 9.6	-37.5	- 8.7	- 3
0.20	0.01	0.19	-19.8	-14.4	- 22.3	-42.1	-13.3	-10
0.10	0.01	0.09	-13.6	-20.9	- 32.4	-46.0	-17.2	-28

Note: $B_0 = 0.10$ MHz

* Arbitrarily chosen as equivalent to $I = 1$ V/MHz.

3) Broadband Measurement System Conclusions

A system for performing broadband measurements of EMI over the range from below 14kHz to above 10 GHz in five bands without tuning has been shown to be physically realizable. The output indication from such a system would be in units, such as decibels, relative to some specification limit. This implies that a threshold detector set at the specification limit would produce a go/no-go indication of the passage or failure of an EMI test of the general type presently required by MIL-STD-461. For such an indication to be meaningful without prior knowledge of the nature of the emissions, all of the ramifications of the measurement specification must be incorporated into the measurement hardware. This will be possible only if a new Broadband Measurement Specification is written around measurement hardware designed to meet certain specific criteria.

The first criteria of importance is frequency response. The Broadband Measurement System is realizable with flat frequency response to conducted emissions over the range 14kHz (or below) to 10 GHz (and above). This flat conducted response can then be translated to radiated response by superimposing broadband antenna factors which, because of physical limitations on antennas, will dictate the shape of the specification curves for radiated emissions. At the present state-of-the-art, antennas may be physically realized with flat antenna factors up to 100MHz (active antennas) and with antenna factors which increase at the rate of 6dB/octave (constant gain) above 100MHz. Once band edges have been established (the band edges in the hypothetical Broadband Measurement System occur at 14kHz, 0.1, 1, 4, 7 and 10GHz), they will have to be standardized so that consistent results can be obtained when measuring broadband emissions which overlap the band edges.

The second criteria of importance is the ratio of narrow-band to broadband responses. This ratio can be specified for CW

and impulse signals and controlled by adjusting the ratio of pre-detection to post-detection bandwidth in a crystal-video receiver. The approximate bandwidths required can be calculated using equations presented herein. The actual system must incorporate adjustable post-detection bandwidths so that thresholds can be accurately set to CW and impulse signals during calibration. The responses to other types of signals should then fall into place. Digital filtering in a microcomputer would be ideal for the final bandwidth adjustment.

The third criteria of importance is dynamic range. The Broadband Measurement System should accept any type of signal for which there is a narrowband or broadband specification limit, at the level corresponding to the limit, without saturation. Failure to do so will result in the system ignoring emissions which exceed the limit. Current technology in the area of low-1/f-noise Schottky-diode detectors is such that this criteria can probably be met for the worst case (impulses) with $r=20\text{dB}$ up to 1GHz, which is as high in frequency as current MIL-STD-461 carries broadband limits. Above 1GHz, the system saturation point should be standardized so that consistent measurements can be made with varying hardware embodiments on marginally-broadband emissions.

While the three basic criteria outlined above are of primary importance, secondary criteria such as sensitivity, false alarm rate (primarily a problem of adequate signal-to-noise ratios, can be reduced by microcomputer analysis) and accuracy (continuous automatic calibration is recommended) are also important. A breadboard Broadband Measurement System should now be assembled and tested to demonstrate feasibility.

B EVALUATION OF MIL-STD-461A LIMITS AND MEASUREMENT PROCEDURE

1) Background

There are twenty-four separate EMI/EMC tests that are required by MIL-STD-461A. Not all of the twenty-four tests are required for all classes of equipment. There are four major class divisions of equipments defined by MIL-STD-461A. They are: Class I, Communications and Electronics (C&G) Equipments; Class II, Non Communication Equipments; Class III, Vehicle and Engine-Driven Equipment; and Class IV, Overhead Power Lines. Each of the classes are divided into sub classes with the exception of Class IV. For the work being performed in this contract, the class of equipment category that describes the type of equipment under consideration is Class IIIA. This class would cover tanks, armored personnel carrier, shelters, helicopters, etc. All of the equipment that would be installed within the Class IIIA System would be either Class I or Class II types.

2) Class IIIA Systems

Of the twenty-four MIL-STD-461A tests only two are required for Class III A equipments. They are CE03 (.02 to 50MHz and RE05 (150KHZ to 1GHZ). These two tests measure the impact that the system has on the environment. There is no provision for susceptibility testing or for intra-system EMI/EMC testing under MIL-STD-461A. The type of testing required for Class III A equipments CE03 and RE05 lends itself well to automated and broadband measurement techniques for testing.

3) Class I and Class II Equipments

The class III A will contain any number of Class I and Class II equipments. The Class I equipments are communication electronic types and will include receiver, transmitter, test equipment, computers, etc. Class II equipments are non communication electrical equipment such as power supplies, motors, power tools, pumps, heaters, etc. Each Class I and Class II equipment is tested in accordance with MIL-STD-461A. Table 11 lists all of the MIL-STD-461A measurements required for Class I and Class II equipments. In order to perform an adequate IEMCAP or similar analysis program on

Table 11. MIL-STD-461A Requirements for Class I and Class II Equipments.

MIL-STD-461A TEST	REQUIRED FOR EQUIPMENT		REMARKS
	CLASS I	CLASS II	
<u>CE01</u> : Conducted Emission Power Leads: 30 Hz - 20 kHz	YES	NO ①	① Yes for power supplies, heaters, and some tools.
<u>CE02</u> : Conducted Emission Control and Signal Leads: 30 Hz - 20 kHz	YES	NO ①	
<u>CE03</u> : Conducted Emission Power Leads: 20 kHz - 50 MHz	YES	YES	
<u>CE04</u> : Conducted Emission Control and Signal Leads: 20 kHz - 50 MHz	YES	NO ①	
<u>CE05</u> : Conducted Emission Inverse Filter Method: 30 Hz - 50 MHz	YES	YES ②	② No for vehicle accessories.
<u>CE06</u> : Antenna Terminal Emissions: 10 kHz - 12.4 GHz	YES ③	NO	③ No for nonantenna equipment.
<u>CS01</u> : Power Lead Susceptibility: 30 Hz - 50 kHz	YES	NO	
<u>CS02</u> : Power Lead Susceptibility: 50 kHz - 400 MHz	YES	NO	
<u>CS03</u> : Conducted Susceptibility Intermodulation: 30 Hz - 10 GHz	YES ④	NO	④ No for transmitter and nonantenna equipments.
<u>CS04</u> : Conducted Susceptibility Rejection of Undesired Signal (Two Sig. Gen. Method): 30 Hz - 10 GHz	YES ④	NO	
<u>CS05</u> : Conducted Susceptibility Cross Modulation: 30 Hz - 10 GHz	YES ④	NO	
<u>CS06</u> : Conducted Susceptibility Spike Power Leads:	YES	NO	
<u>CS07</u> : Conducted Susceptibility Squelch Circuits:	YES ⑤	NO	⑤ No for transmitting equipment - applies to receivers with squelch circuits only.
<u>CS08</u> : Conducted Susceptibility Rejection of Undesired Signal (One Sig. Gen. Method): 30 Hz - 10 GHz	YES ④	NO	
<u>RE01</u> : Radiated Emission Magnetic Field: 30 Hz - 30 kHz	YES ⑥	NO ①	⑥ No for nonantenna equipments.
<u>RE02</u> : Radiated Emission Electric Field: 14 kHz - 10 GHz	YES	YES	
<u>RE03</u> : Radiated Emission Spurious and Harmonics Radiated Technique: 10 kHz - 40 GHz	YES ⑦	NO	⑦ Applies to transmitting equipment only.
<u>RE04</u> : Radiated Emission Magnetic Field: 20 Hz - 50 kHz	YES ③	NO ①	
<u>RE05</u> : Radiated Emission Vehicles and Engine-Driven Equipment: 150 kHz - 1 GHz	NO	NO	
<u>RE06</u> : Radiated Emission Overhead Power Line Test	NO	NO	
<u>RS01</u> : Radiated Susceptibility Magnetic Field: 30 Hz - 30 kHz	YES	NO	
<u>RS02</u> : Radiated Susceptibility Magnetic Induction Field	YES	NO	
<u>RS03</u> : Radiated Susceptibility Electric Field: 14 kHz - 10 GHz	YES	NO	
<u>RS04</u> : Radiated Susceptibility Electric Field: 14 kHz - 30 MHz	YES	NO	

a Class III A equipment, data from some of these tests should be available as data inputs. Table 12 lists the MIL-STD-461A tests now used by IEMCAP as data inputs. It also evaluates the suitability of applying an automated or broadband measurement technique to the measurement procedures to produce this data.

4) Intra System Testing and Analysis

The EMI/EMC analysis of a Class III A equipment may begin during its design stages; even as early as concept design. The EMI/EMC data requirements for the individual Class I and Class II equipments to be part of the Class III A equipment will be defined by the requirements of the EMI/EMC Analysis system to be used. If IEMCAP is used then, as a minimum the data listed in Table 12 as IEMCAP inputs should be known for the analysis. Once the EMI/EMC analysis is run then design decision may be made with respect to equipment selection, placement and installation. The analysis will identify critical positions and frequencies within the system. From the results of the analysis an EMI/EMC intra-system test plan may be written for the equipment in its final configuration. The test plan will concentrate on identified problem areas and will not necessarily be held to MIL-STD-461A limits. Automated and/or broadband measurement techniques shall be utilized to expedite the measurement program. The results of the measurement program will not be how well emission levels compare to some limit level but rather that the emission levels are below the threshold susceptibility level of any equipment in the overall system. This will allow the tailoring of the intrasystem tests and limits to conditions revealed in the analysis phase of the EMI/EMC design. The analysis could also serve as the determining factor as to which MIL-STD-461 A tests should be run on new class I and class II equipments to be part of the system and which limits for the particular test could be relaxed.

Table 12. MIL-STD-461A Data Use in IEMCAP and Measurement Technique Evaluation.

MIL-STD-461A TEST	REQUIRED AS IEMCAP INPUT	MEASUREMENT TECHNIQUE		COST AND DIFFICULTY
		AUTOMATED	BROADBAND	
<u>CE01</u> : Conducted Emission Power Leads: 30 Hz - 20 kHz	NO	YES	YES	LOW
<u>CE02</u> : Conducted Emission Control and Signal Leads: 30 Hz - 20 kHz	YES	YES	YES	LOW
<u>CE03</u> : Conducted Emission Power Leads: 20 kHz - 50 MHz	YES	YES	YES	LOW
<u>CE04</u> : Conducted Emission Control and Signal Leads: 20 kHz - 50 MHz	YES	YES	YES	LOW
<u>CE05</u> : Conducted Emission Inverse Filter Method: 30 Hz - 50 MHz	NO	NO	NO	HIGH *
<u>CE06</u> : Antenna Terminal Emissions: 10 kHz - 12.4 GHz	YES	YES	YES	MEDIUM
<u>CS01</u> : Power Lead Susceptibility: 30 Hz - 50 kHz	YES	YES	NO	LOW
<u>CS02</u> : Power Lead Susceptibility: 50 kHz - 400 MHz	YES	YES	NO	LOW
<u>CS03</u> : Conducted Susceptibility Intermodulation: 30 Hz - 10 GHz	NO	NO	NO	HIGH
<u>CS04</u> : Conducted Susceptibility Rejection of Undesired Signal (Two Sig. Gen. Method): 30 Hz - 10 GHz	NO	NO	NO	HIGH
<u>CS05</u> : Conducted Susceptibility Cross Modulation: 30 Hz - 10 GHz	NO	NO	NO	MEDIUM
<u>CS06</u> : Conducted Susceptibility Spike Power Leads:	NO	YES	YES	LOW
<u>CS07</u> : Conducted Susceptibility Squelch Circuits:	NO	NO	NO	LOW
<u>CS08</u> : Conducted Susceptibility Rejection of Undesired Signal (One Sig. Gen. Method): 30 Hz - 10 GHz	NO	YES	NO	MEDIUM
<u>RE01</u> : Radiated Emission Magnetic Field: 30 Hz - 30 kHz	NO	YES	YES	LOW
<u>RE02</u> : Radiated Emission Electric Field: 14 kHz - 10 GHz	YES	YES	YES	MEDIUM
<u>RE03</u> : Radiated Emission Spurious and Harmonics Radiated Technique: 10 kHz - 40 GHz	NO	YES	YES	HIGH
<u>RE04</u> : Radiated Emission Magnetic Field: 20 Hz - 50 kHz	NO	YES	YES	LOW
<u>RE05</u> : Radiated Emission Vehicles and Engine-Driven Equipment: 150 kHz - 1 GHz	NO	YES	YES	MEDIUM
<u>RE06</u> : Radiated Emission Overhead Power Line Test	NO	YES	YES	LOW
<u>RS01</u> : Radiated Susceptibility Magnetic Field: 30 Hz - 30 kHz	NO	SEMI	NO	LOW
<u>RS02</u> : Radiated Susceptibility Magnetic Induction Field	NO	SEMI	NO	LOW
<u>RS03</u> : Radiated Susceptibility Electric Field: 14 kHz - 10 GHz	YES	SEMI	NO	HIGH
<u>RS04</u> : Radiated Susceptibility Electric Field: 14 kHz - 30 MHz	YES	SEMI	NO	MEDIUM

* Usually performed in lieu of CE01, CE02, CE03, and CE04.

4. WORK PLANNED FOR THE FOURTH QUARTER

In the fourth quarter a number of technical areas of investigation must be completed. This will include the review of measurement techniques and instrumentation for frequencies above 10 GHz, description and evaluation of existing automated EMI/EMC test systems and the completion of the evaluation of the MIL-STD-461A limits and MIL-STD-462 test procedures. The results of this work will be combined with the work done in the earlier quarters of this contract in a final technical report. The report will also contain a review of all the goals of the contract and how well they were met.

DISTRIBUTION LIST

<u>Address</u>	<u>No. of Copies</u>
Defense Technical Information Center ATTN: DTIC-TCA Cameron Station (Bldg 5) Alexandria, VA 22314	12
Director National Security Agency ATTN: TDL Fort George G. Meade, MD 20755	01
DCA Defense Communications Engineering Center CODE R123, Tech Library 1860 Wiehle Avenue Reston, VA 20090	01
Defense Communications Agency Technical Library Center CODE 205 (P.A. TOLOVI) Washington, DC 20305	02
Commanding Officer Naval Research Laboratory ATTN: CODE 2627 Washington, DC 20375	01
Commander Naval Ocean Systems Center ATTN: Library San Diego, CA 92152	01
Commander Naval Surface Weapons Center White Oak Laboratory ATTN: Library, CODE WX-21	01
Commandant Marine Corps ATTN: CODE LMC Washington, DC 20380	02
Headquarters US Marine Corps ATTN: CODE INTS Washington, DC 20380	01

DISTRIBUTION LIST (CONTD)

<u>Address</u>	<u>No. of Copies</u>
Command, Control & Communications Division Development Center Marine Corps Development & Education Command Quantico, VA 22134	01
Naval Telecommunications Command Technical Library, CODE 9IL 4401 Massachusetts Avenue, NW Washington, DC 20390	01
Naval Air Systems Command CODE: AIR-5332 Washington, DC 20360	04
Dr. T. G. Berlincourt Office of Naval Research (CODE 420) 800 N. Quincy Street Arlington, VA 22217	01
AUL/LSE 64-285 Maxwell AFB, AL 36112	01
Rome Air Development Center ATTN: Documents Library (TSLD) Griffiss ARB, NY 13441	01
USAFETAC/CBTL ATTN: Librarian STOP 825 Scot AFB, IL 62225	01
Air Force Geophysics Lab L. G. Hanscom AFB ATTN: LIR Bedford, MA 01730	01
AFGL/SULL S-29 HAFB, MA 01731	01
Headquarters AFEWC ATTN: EST San Antonio, TX 78243	02

DISTRIBUTION LIST (CONTD)

<u>Address</u>	<u>No. of Copies</u>
Headquarters Air Force Systems Command ATTN: DLWA/Mr. P. Sandler Andres AFB Washington, DC 20331	01
Commander MIRCOM Redstone Scientific Information Center ATTN: Chief, Document Section Redstone Arsenal, AL 35809	02
Commander MIRCOM ATTN: DRSMI-RE (Mr. Pittman) Redstone Arsenal, AL 35809	01
Commandant US Army Aviation Center ATTN: ATZQ-D-MA Fort Rucker, AL 36362	01
Commander Headquarters Fort Huachua ATTN: Technical Reference Division Fort Huachua, AZ 85613	01
Commander US Army Electronic Proving Ground ATTN: STEEP-MT Fort Huachuca, AZ 85613	01
Commander US Army Proving Ground ATTN: STEYP-MTD (Tech Library) Yuma, AZ 85364	01
Director US Army Air Mobility R&D Lab ATTN: T. Gossett, Bldg 207-5 Nasa Ames Research Center Moffett Field, CA 94035	01
HQDA (DAMO-TCE) Washington, DC 20310	02

DISTRIBUTION LIST (CONTD)

<u>Address</u>	<u>No. of Copies</u>
Deputy For Science & Technology Office, Asst Sec Army (R&D) Washington, DC 20310	02
HQDA (DAMA-ARZ-D/Dr. F. D. Verderame) Washington, DC 20310	01
Commandant US Army Signal School ATTN: ATSH-CD-MS-E Fort Gordon, GA 30905	01
Commandant US Army Infantry School ATTN: ATSH-CD-MS-E Fort Benning, GA 31905	01
Commander ARRCOM ATTN: Systems Analysis Office, DRSAR-PE Rock Island, IL 61299	01
Director, Combat Developments US Army Armor Center ATTN: ATZK-CD-MS Fort Knox, KY 40121	02
Commander US Army Test & Evaluation Command ATTN: DRSTE-CT-C Aberdeen Proving Ground, MD 21005	01
Commander Harry Diamond Laboratories ATTN: Library 2800 Powder Mill Road Adelphi, MD 20783	01
Director US Army Ballistic Research Labs ATTN: DRXBR-LB Aberdeen Proving Ground, MD 21005	01

DISTRIBUTION LIST (CONTD)

<u>Address</u>	<u>No. of Copies</u>
Director US Army Human Engineering Labs Aberdeen Proving Ground, MD 21005	01
Director US Material Systems Analysis Activity ATTN: DRXSY-T Aberdeen Proving Ground, MD 21005	01
Director US Army Material Systems Analysis Activity ATTN: DRXSY-MP Aberdeen Proving Ground, MD 21005	01
Chief CERCOM Aviation Electronics Office ATTN: DRSEL-MME-LAF(2) St. Louis, MO 63166	01
Commander AVRADCOM ATTN: DRSAY-E PO Box 209 St. Louis, MO	01
Commander ARRADCOM ATTN: DRDAR-LIN-S (Bldg 95) Dover, NJ 07801	01
Commander ARRADCOM ATTN: DRDAF-TSS, #59 Dover, NJ 07801	01
Director Joint Communication Office (TRI TAC) ATTN: TT-AD (Tech Doc Cen) Fort Monmouth, NJ 07703	01
PM, FIREFINDER/REMBASS ATTN: DRCPM-FER Fort Monmouth, NJ 07703	01
Commander ERADCOM ATTN: DELSO-L ATTN: DELSO-L-S Ft. Monmouth, NJ 07703	01 02

DISTRIBUTION LIST (CONTD)

<u>Address</u>	<u>No. of Copies</u>
Project Manager NAVCON ATTN: DRCPM-NC-TM Fort Monmouth, NJ	01
Commander US Army Satellite Communications Agency ATTN: DRCPM-SC-3 Fort Monmouth, NJ 07703	02
TRI-TAC Office ATTN: TT-SE Fort Monmouth, NJ 07703	01
Commander US Army Avionics Lab AVRADCOM ATTN: DAVAA-D Fort Monmouth, NJ 07703	01
Commander US Army Research Office ATTN: Dr. Horst Wittmann PO Box 12211 Research Triangle Park, NC 27709	01
Commander US Army Research Office ATTN: DRXRO-IP PO Box 12211 Research Triangle Park, NC 27709	02
Commander US Army Research Office ATTN: DRXRO-PH (Dr. R. J. Lontz) Research Triangle Park, NC 27709	02
Commandant US Army Inst For Military Assistance ATTN: ATSU-CTD-MO Fort Bragg, NC 28307	02
Commandant USAFAS ATTN: ATSF-CD-DE Fort Sill, OK 73503	01

DISTRIBUTION LIST (CONTD)

<u>Address</u>	<u>No. of Copies</u>
Commandant US Army Air Defense School ATTN: ATSA-CD-MS-C Fort Bliss, TX 79916	01
Commander DARCOM ATTN: DRCDE 5001 Eisenhower Avenue Alexandria, VA 22333	01
Commander US Army Signals Warfare Lab Vint Hill Farms Station Warrenton, VA 22186	02
Commander US Army Signals Warfare Lab ATTN: DELSW-AO Vint Hill Farms Station Warrenton, VA 22186	01
Commandant US Army Engineer School ATTN: ATZA-TDL Fort Belvoir, VA 22060	02
Commander US Army Engineer Topographic Labs ATTN: ETL-TD-EA Fort Belvoir, VA 22060	01
Commander US Army Logistics Center ATTN: ATCL-MC Fort Lee, VA 22801	02
Commander TRADOC ATTN: TDOC-TA Fort Monroe, VA 23561	01
Commander US Army Training & Doctrine Command ATTN: ATCD-TM Fort Monroe, VA 23561	01

DISTRIBUTION LIST (CONTD)

<u>Address</u>	<u>No. of Copies</u>
Commander US Army Garrison Vint Hill Farms Station ATTN: IAVAAF Warrenton, VA 22186	01
Project Manager Control & Analysis Centers Vint Hill Farms Station Warrenton, VA 22186	01
Commander Night Vision & Electro-Optics Lab ERADCOM ATTN: DELNV-D Fort Belvoir, VA 22060	01
Commander Atmospheric Sciences Lab ERADCOM ATTN: DELAS-SY-S White Sands Missile Range, NM 83002	01
Chief Office Missile Electronic Warfare Electronic Warfare Lab, ERADCOM White Sands Missile Range, NM 88002	01
Chief Intel Material Development & Support Office Electronic Warfare Lab, ERADCOM Fort George G. Meade, MD 20755	01
Commander US Army Ballistic Research Lab/ARRADCOM ATTN: DRDAR-TSB-S (ST INFO) Aberdeen Proving Ground, MD 21005	01
Commander ERADCOM ATTN: DRDEL-CT 2800 Powder Mill Road Adelphi, MD 20783	02
Commander ERADCOM ATTN: DRDEL-PA 2800 Powder Mill Road Adelphi, MD 20783	01

DISTRIBUTION LIST (CONTD)

<u>Address</u>	<u>No. of Copies</u>
Headquarters Harry Diamond Laboratories ATTN: DELHD-TD (Dr. W. W. Carter) 2800 Powder Mill Road Adelphi, MD 20783	01
MIT - Lincoln Laboratory ATTN: Library (RM A-082) PO Box 73 Lexington, MA 02173	01
NASA Scientific & Tech Information Facility Baltimore/Washington Intl Airport PO Box 8757, MD 21240	01
National Bureau of Standards Bldg 225, RM A-331 ATTN: Mr. Leedy Washington, DC 20231	01
Dr. Clayton Paul Electrical Engineering Dept University of Kentucky Lexington, KY 40506	01
Mr. John Spina RADC/RBCT Griffiss AFB, NY 13441	01
Commander US Army Communications Research & Development Command ATTN: DRDCO-SEI-A/Mr. Sam Segner Fort Monmouth, NJ 07703	01
Commander US Army Communications Research & Development Command ATTN: DRDCO-COM-D Fort Monmouth, NJ 07703	01
Commander US Army Communications Research & Development Command ATTN: DRDCO-COM-RY-3/Mr. Stuart Albert Fort Monmouth, NJ 07703	15

FILMED

7-8